Aalborg Universitet

AALBORG UNIVERSITY
DENMARK

A Self-Contained Cylinder Drive with Indirectly Controlled Hydraulic Lock

Ketelsen, Søren; Andersen, Torben Ole; Ebbesen, Morten Kjeld; Schmidt, Lasse

Published in:
Modeling, Identification and Control (Online)

DOI (link to publication from Publisher):
10.4173/mic.2020.3.4

Creative Commons License
CC BY 3.0

Publication date:
2020

Document Version
Publisher's PDF, also known as Version of record

Link to publication from Aalborg University

Citation for published version (APA):
Ketelsen, S., Andersen, T. O., Ebbesen, M. K., & Schmidt, L. (2020). A Self-Contained Cylinder Drive with Indirectly Controlled Hydraulic Lock. *Modeling, Identification and Control (Online)*, *41*(3), 185-205. https://doi.org/10.4173/mic.2020.3.4

General rights
Copyright and moral rights for the publications made accessible in the public portal are retained by the authors and/or other copyright owners and it is a condition of accessing publications that users recognise and abide by the legal requirements associated with these rights.

- Users may download and print one copy of any publication from the public portal for the purpose of private study or research.
- You may not further distribute the material or use it for any profit-making activity or commercial gain
- You may freely distribute the URL identifying the publication in the public portal -

Take down policy
If you believe that this document breaches copyright please contact us at vbn@aub.aau.dk providing details, and we will remove access to the work immediately and investigate your claim.

Downloaded from vbn.aau.dk on: May 05, 2023

Modeling, Identification and Control, Vol. 41, No. 3, 2020, pp. 185–205, ISSN 1890–1328

A Self-Contained Cylinder Drive with Indirectly Controlled Hydraulic Lock

S. Ketelsen [1] T.O. Andersen [1] M.K. Ebbesen [2] L. Schmidt [1]

[1] *Department of Energy Technology, Aalborg University, 9220 Aalborg, Denmark. E-mail:* sok@et.aau.dk

[2] *Department of Engineering Sciences, University of Agder, Grimstad, Norway*

Abstract

This paper presents a self-contained pump-controlled hydraulic linear drive including an innovative load holding sub-circuit. For safety critical applications such as crane manipulators, locking valves or load holding valves are enforced by legislation, but the load holding functionality may also be used actively to decrease the energy consumption for applications where the load is kept stationary for longer periods of time. The system proposed in this paper is based on a simple hydraulic architecture using two variable-speed electric motors each connected to a fixed-displacement pump. This architecture is well-known in academic literature, but in this paper a novel load holding sub-circuit has been included. To control this load holding functionality, the low chamber pressure needs to be controlled accurately, while still being able to control the motion of the cylinder piston as well. Due to strong cross-couplings between cylinder piston motion and chamber pressures this task is non-trivial. The control for opening the locking valves is indirect in the sense that it is controlled via the chamber pressures, which are actively controlled. The fundamental control strategy presented in this paper is based on transforming the highly coupled physical states to virtual states, significantly reducing cross-couplings.

As a case study, a two link medium sized knuckle boom crane is selected as an application example. Simulation results confirm the applicability of the proposed system. Appropriate position tracking performance has been achieved for the considered motion trajectory, while the low chamber pressure is controlled in a satisfying manner. A smooth transition from motion operating mode to load holding mode is achieved, with the system not requiring any input energy to keep the load stationary when the hydraulic cylinder lock is engaged.

Keywords: Energy efficient hydraulic actuation, pump-controlled cylinder, cylinder direct drive, multi-variable control, load holding, safety functionality, cylinder lock

1 Introduction

Hydraulic linear actuation technology is well-known for its high power and force densities. This often makes the technology the preferred solution for applications characterised by low speed high force operation. Such applications may include large industrial machinery, e.g. presses, test-equipment, construction machines, and cranes. In many industries the preferred linear hydraulic actuator is the standard differential cylinder (Quan et al., 2014; Weber et al., 2016). Conventionally, several cylinders are supplied from a centralised hydraulic power unit (HPU), and individual valves control the motion of each cylinder by throttling the chamber flows. The resulting pressure loss inherently leads to a poor energy efficiency of conventional hydraulic systems. To improve the energy efficiency, a load sensing HPU is often utilised. Here the supply pressure is adjusted to the needs of the cylinder requiring the

doi:10.4173/mic.2020.3.4

© 2020 Norwegian Society of Automatic Control

largest pressure, which reduces the throttling losses, especially if the pressure level is similar for all consumers. In situations where a slowly moving consumer requires a high supply pressure, while a fast moving consumer requires a low supply pressure, significant pressure losses are however still present.

To significantly increase the energy efficiency, the throttle based control clearly needs to be eliminated, while preserving controllability, still at a reasonable cost level. An obvious idea is to completely replace the hydraulic technology with a competing technology, such as electro-mechanical drives, e.g. ball or roller screws. Due to low reliability under high load conditions (e.g. shock load damage) and limited force capabilities this technology is not well-suited for all applications (Hagen et al., 2017; Padovani et al., 2019).

Another idea is to stay with the hydraulic technology and the centralised HPU, and replace the control valve with other components. The so-called digital hydraulic technology is one approach for doing so. One branch of digital hydraulics considers multi-chamber cylinders. Here the conventional control valve is replaced by several on/off valves which may be supplied by multiple pressure lines (Hedegaard Hansen et al., 2017; Linjama et al., 2003; Hedegaard Hansen and Pedersen, 2016; Hedegaard Hansen et al., 2018). In Donkov et al. (2017, 2018) a simulation study investigating actuation of a knuckle boom crane using the digital hydraulic technology was conducted. The results show an improved energy efficiency, but an unsatisfying tracking performance due to the discrete valve switching.

Recently, industrial and academic interest into self-contained pump-controlled cylinder drive technology has been increasing. Here the idea is to replace the conventional control valve and the centralised HPU, with one or more electric motors and hydraulic pumps to control each cylinder. This solution holds several benefits compared to conventional control valves. The resistive losses associated with throttling are ideally eliminated, leading to a significantly improved energy efficiency. This is furthermore strengthened because self-contained cylinder drives are generally able to recover energy in aided load situations. Secondly, all components, i.e. cylinder, motors, pumps, pressurised oil tank, hydraulic manifold, are integrated into a single unit, eliminating the need of piping to the centralised HPU.

A general challenge for controlling a differential cylinder directly by the pump flow is to compensate the uneven flow requirements originating from the asymmetry of the cylinder. Two fundamentally different solutions may be found in literature: valve-compensated and pump-compensated architectures (Costa and Sepehri, 2018). A comprehensive overview of both compensation topologies is given in Ketelsen et al. (2019b).

In valve-compensated architectures a single (symmetric) pump is often used, which requires auxiliary valves to handle cylinder flow asymmetry. In Michel and Weber (2012); Hewett (1994); Çalkan et al. (2015) an inverse shuttle valve is used to always connect the low pressure chamber of the cylinder with the low pressure reservoir. In Rahmfeld and Ivantysynova (2001); Padovani et al. (2019); Schneider et al. (2014) this is achieved using pilot-operated check valves. To avoid oscillatory valve switchings - so-called mode oscillation - for certain load situations, Padovani et al. (2020); Gøytil et al. (2020) suggests using actively controlled on/off valves. A common disadvantage of valve-compensated architectures compared to conventional valve-control, is the fact that the pressure in the low pressure chamber is close to the low pressure reservoir. This lowers the drive stiffness which in turn causes the realisable control bandwidth to decrease, and thus limits the application range of these concepts.

The uneven flow requirement may also be compensated by mounting multiple pumps, typically two, on the same shaft. Here the displacement ratio of the pumps must be matched to the cylinder asymmetry. This strategy has been investigated in Pedersen et al. (2014); Brahmer (2012); Minav et al. (2014); Grønkær et al. (2020); Schmidt et al. (2020), where the issues of low pressure operation similar to valve-compensated architectures are also present. To avoid low pressure operation Schmidt et al. (2019b,a), suggested to include rectifying check valves in combination with actively controlled proportional valves. This enables controlling the cylinder flow into the cylinder by the pump and flow from the cylinder using proportional valves.

Another approach to avoid low pressure operation is given in Schmidt et al. (2015, 2017). Here a third pump, only active in the forward direction is included. By advanced control efforts, it was proven experimentally possible, to control the pressure in the low pressure chamber and thus maintain a desired drive stiffness, while in motion. In Ketelsen et al. (2018), this drive concept was used for actuation of a middle sized two link knuckle boom crane. Simulation results suggested a significantly improved energy efficiency compared to a conventional load sensing system. For a real life working trajectory the consumed energy was lowered by 60 %.

The drive concept utilised in Ketelsen et al. (2018) lacked the safety functionality often realised by counter-balance-valves (CBV) in conventional systems, i.e. a flow-blocking device ensuring that in case of power shutdown or overrunning loads controllability of the load is not lost. This is done by ensuring that a cer-

tain back pressure is always present during operation. In pump-controlled systems CBV's may be utilised as well. CBV's are however throttling devices, meaning that these typically reduce the achievable energy efficiency and may preclude the opportunity of energy recovery in certain load situations (Imam et al., 2017; Jalayeri et al., 2015).

Cylinder locking or load holding may also be achieved by installing pilot-operated check valves or logic elements in the main transmission lines. As shown in Padovani et al. (2019), this may lead to undesired oscillatory valve openings and piston motion, for some configurations of the pilot-operated check valves. In Hagen et al. (2018) and Schneider et al. (2014) the pilot pressure is controlled using an electrically actuated on/off valve which avoids oscillatory check valve openings.

Due to a desire of keeping safety functionality in hydraulic/mechanical components, without compromising energy efficiency and controllability an innovative load holding concept is presented in this paper. The functionality of this circuit is based upon the requirement that the low chamber pressure may be controlled rather accurately for all operating scenarios. Therefore the triple pump concept, investigated by the authors in Ketelsen et al. (2018) is found infeasible.

Instead a circuit architecture based on two variable-speed electrical prime movers, each connected to a fixed-displacement pump is utilised. This gives the required controllability, being able to control both piston motion and the lower chamber pressure. This dual variable-speed pump drive is abbreviated DvSP in the following. Using two prime movers increases the scalability of the drive, which may be important for applications requiring large actuator powers, such as crane manipulators (Ketelsen et al., 2019a; Gøytil et al., 2019). The idea of using two variable flow suppliers is not new. For variable-displacement pumps this is found in Dantlgraber (1993); Feuser et al. (1995); Lodewyks (1994). For two variable-speed prime movers this is considered in Helduser (1999); Neubert (2002). However none of the mentioned references consider controlling a load holding device in combination with two prime movers.

This paper is organized in the following order: In the next section the hydraulic system is presented. In section 3 an application example chosen as a knuckle boom crane is presented. The hydraulic architecture has a wide application range, but a knuckle boom crane is found to be a well suited application, due to the requirement of safety/load holding functionality and the need of four quadrant operation including smooth switching between quadrants. In section 4 and 5 nonlinear and linear models are derived and an analysis of the input-output cross couplings is presented. Based on the results of the coupling analysis, a control strategy based on state decoupling is derived in section 6 and 7. In section 8 simulation results are presented.

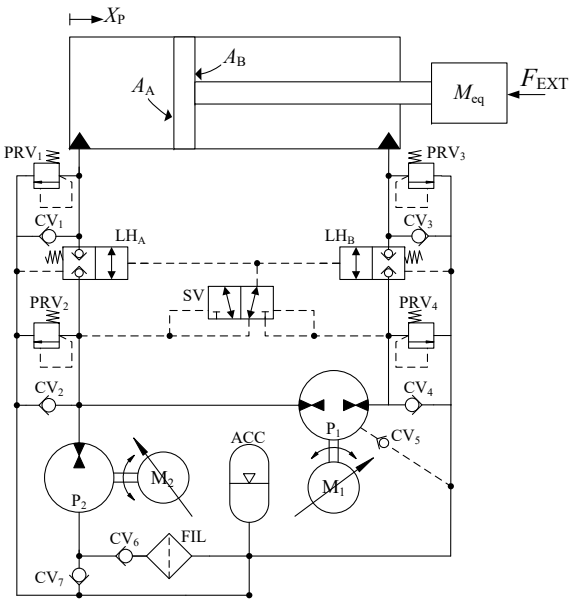

Figure 1: Asymmetric cylinder controlled by the dual variable-speed pump (DvSP) system.

2 Pump-Controlled Cylinder Drive with Self-Locking Ability

The proposed DvSP drive is shown in Fig. 1. The concept consists of a closed-circuit pump, P_1, which is connected to both cylinder chambers and driven by the variable-speed electric machine M_1. An open circuit pump P_2 is driven by the variable-speed electric machine M_2 and provides uneven chamber flow compensation. A pressurized accumulator is used for storing the cylinder rod volume, compression volume and thermal expansion volume. To keep the reservoir pressure low, a large gas volume is needed. For the current study a gas volume of 288 L is used. Recently Ketelsen et al. (2020a,b) suggested implementing a gasless reservoir in pump-controlled systems to increase system compactness. For filtering a hydraulic filter is included. Check valves CV_6 and CV_7 ensure uni-directional filter flow. The valves LH_A and LH_B are used to lock the cylinder. These valves are closed unless the pilot pressure is high enough to open the valve against the spring force. The pilot pressure is controlled using the inverse shuttle valve, SV, which is supplying the lowest chamber pressure to the pilot line. To avoid undesired loss of pilot pressure the shuttle valve must switch in open

rather than closed transition. If the lowest chamber pressure is controlled appropriately, oscillatory openings of the load holding valves may be avoided. The three valves LH_A, LH_B and SV constitute the cylinder lock/load holding sub-circuit and ensure that the hydraulic cylinder is locked if the lowest pressure is not controlled to be larger than the opening pressure of LH_A, LH_B. In case of hose leak, power cut-off or similar emergency the load is going to move slightly until the volume increase in one of the chambers causes the pressure to decrease, in turn causing the load holding valves to close. This effectively locks the cylinder piston and load. On the other hand, if the lowest chamber pressure is successfully controlled to be larger than the full open pressure of the load holding valves, the cylinder piston is unlocked and controllable. Please note that the load holding valves should be sized, such that the pressure drop at full cylinder flow is small.

2.1 Operation Modes

In Fig. 2 a simplified schematics of the DvSP drive is shown in motion operating mode (a) to (d) and in self-locking/load holding mode (e) and (f). The desired operation modes are described in the following.

2.1.1 Four Quadrant Motion Operation Mode

In the four operating quadrants given in Fig. 2 the lower chamber pressure is controlled to ensure that the load holding valves are fully open. Notice that in the figure, chamber pressures and their adjacent transmission lines are the same color to indicate that the pressure drop across the load holding valves in motion operating mode is considered negligible.

In the first quadrant, Fig. 2a, the external load prescribes the piston side chamber pressure P_A to be larger than the rod side chamber pressure P_B, such that P_B is controlled to ensure the load holding valves are fully open. The cylinder is extending meaning that pump 1 is moving oil from the rod chamber to the piston chamber while pump 2 is delivering fluid from the accumulator to the piston side chamber. Both motors are supplying energy to the system in this quadrant. If the cylinder area ratio is 0.5, the two pumps need to supply the same amount of flow statically.

In the second quadrant Fig. 2b, the cylinder retracts under an assistive load. Both motors act as generators in this operating quadrant and a potential for recovering some of the energy supplied by the load exists.

In the third and fourth quadrant the external load prescribes $P_B > P_A$. An important difference from quadrant 1 and 2, is the fact that the operation mode of the electric machines is not identical. For example in the third quadrant, motor 1 is supplying energy to

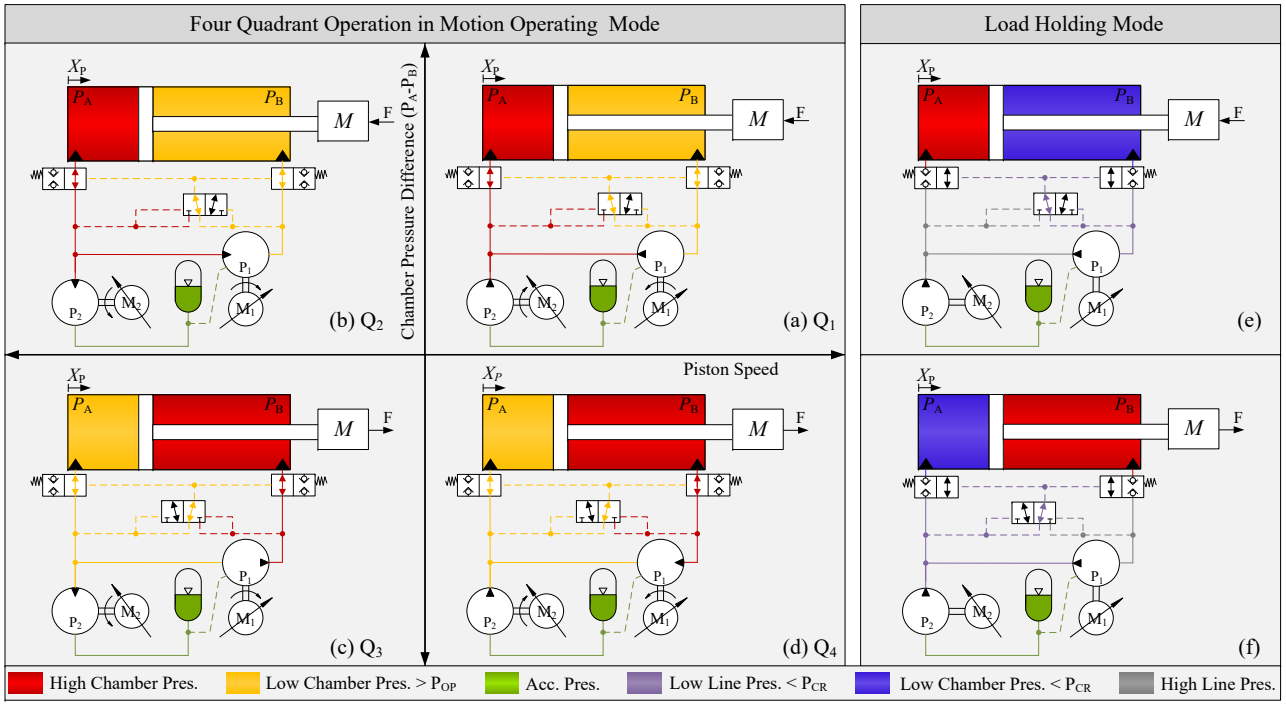

Figure 2: Four quadrant operation schematics of a asymmetric cylinder controlled by the DvSP-system.

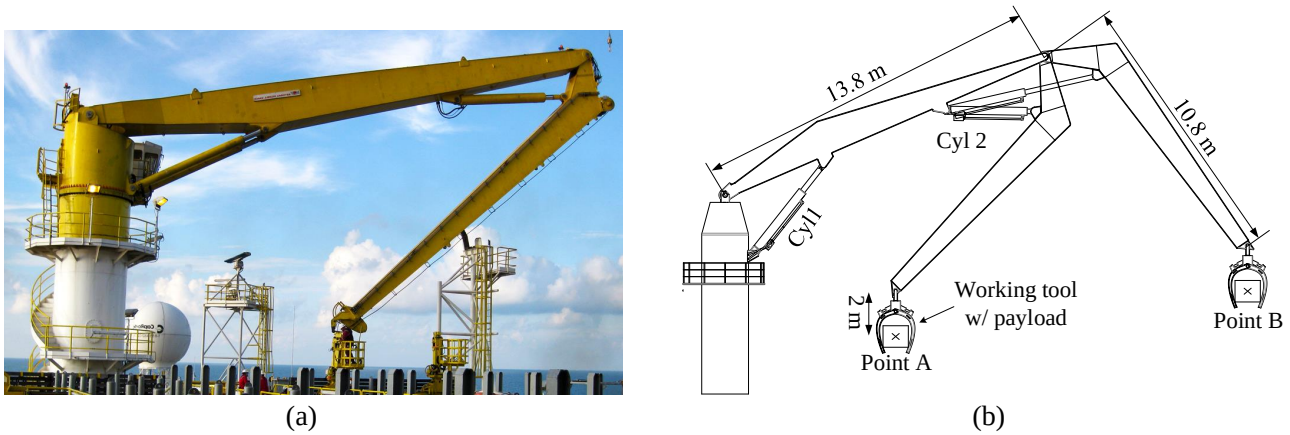

Figure 3: (a) Example of knuckle boom crane with two links provided by National Oilwell Varco ©; (b) Simplified drawing of the knuckle boom crane used as a case study. The considered motion trajectory in tool center space is indicated.

the system while motor 2 is in generator mode. The opposite is true in the fourth quadrant. This situation arises, because the pressure in the low pressure chamber is required to be above the accumulator pressure, to open the load holding valves. If this was not desired, motor 2 would be idling in quadrants 3 and 4. For operation in the third and fourth quadrant, it is beneficial to have a shared DC supply to the frequency converters controlling the motion of the two motors. This would facilitate that the power generated by one motor, may be supplied directly to the other motor.

2.1.2 Load Holding Mode

In load holding mode, Fig. 2e and 2f, the smallest transmission line pressure is below the cracking pressure of the load holding valves, such that these are fully closed. This means that the cylinder piston is hydraulically locked. In the case of emergency i.e. power loss or hose burst, the lowest chamber pressure cannot be kept above the opening pressure of the load holding valves, meaning that the system enters this operation mode. The load holding mode may also be engaged actively during nominal operation to save energy in stationary situations. In these situations it is obviously beneficial to control the pressure in the transmission lines to equal the accumulator pressure to yield zero torque on the pump shafts.

3 Application Example

A relevant application for studying the DvSP drive is the actuation of crane manipulators. During emergencies e.g. power-shutdown or hose burst, the load needs to be locked passively by hydraulically and/or mechanically actuated components. Furthermore, the power requirements for large crane manipulators may be sub-

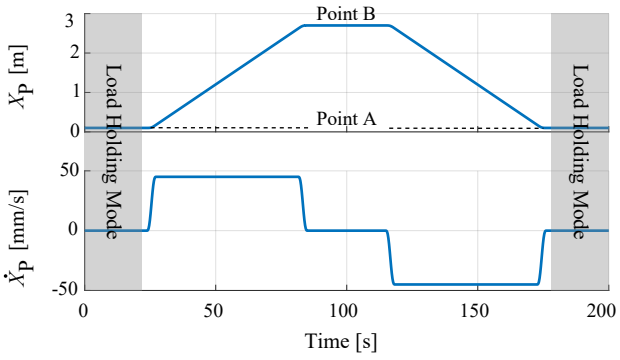

Figure 4: Considered motion trajectory in actuator space.

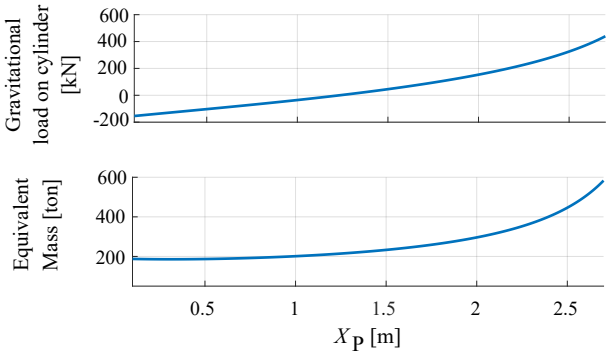

Figure 5: Actuator loads for DvSP system as a function of piston position X_P.

stantial, meaning that sharing this between two electrical prime movers improves the scalability compared to single prime mover architectures.

To show the applicability of the proposed system architecture, a medium sized knuckle boom crane similar to the one shown in Fig. 3 is selected as a case study.

For the study presented in this paper, the knuckle boom actuator (cylinder 2) is considered for actuation by the DvSP drive, while the main actuator (cylinder 1) is kept stationary. This is chosen to keep focus on main functionality and control of the hydraulic architecture, rather than control and performance on the machine level (crane). Using the knuckle boom actuator as a case study is suitable, since this requires operation in all four operating quadrants (see Fig. 2). Furthermore the DvSP drive is commanded to enable load holding mode at point A, meaning that the transition back and forth between motion and load holding mode is tested as well. The considered trajectory in actuator space is given in Fig. 4

Seen from the actuator perspective the trajectory may be considered an *advanced* drive task, due to the four operation quadrants, enabling/disabling of the load holding functionality and the large parameter variations typical for actuating a crane manipulator (See Fig. 5).

For brevity, it has been decided to focus on how the DvSP drive performs under such demanding conditions rather than focusing on modelling/parametrisation of a specific crane. Therefore it has been chosen to use a dynamic mechanical model of the considered crane (Fig. 3b) that was derived by the authors in Ketelsen et al. (2018). Here it suffices to show the equivalent inertia and gravitational load (see Fig. 5) experienced by the knuckle boom actuator, when performing the motion trajectory shown in Fig. 3b and Fig. 4. The velocity dependent forces (e.g. Coriolis forces) are not shown in Fig. 5, due to insignificance compared to the gravitational load.

4 Mathematical Model of the DvSP Drive

During nominal operation of the DvSP drive the pressure relief valves PRV_1 to PRV_4 and the check valves CV_1 to CV_4 in Fig. 1 are closed at all times. By further assuming CV_5 to CV_7 and the filter (FIL) to be ideal the hydraulic schematic in Fig. 1 may be reduced to the one depicted in Fig. 6, and used for deriving the non-linear system model.

Considering Fig. 6, the DvSP system is modelled by Eq. (1)-(18). Cylinder cross port leakage is assumed negligible, and the following definitions are made $V_\mathrm{A} = V_{0\mathrm{A}} + A_\mathrm{A} X_\mathrm{P}$, $V_\mathrm{B} = V_{0\mathrm{B}} - A_\mathrm{B} X_\mathrm{P}$, $\alpha = A_\mathrm{B}/A_\mathrm{A}$. The volumes $V_\mathrm{PB}, V_\mathrm{PA}$, V_PI and V_0 (pipe/hose connection to accumulator) are constant.

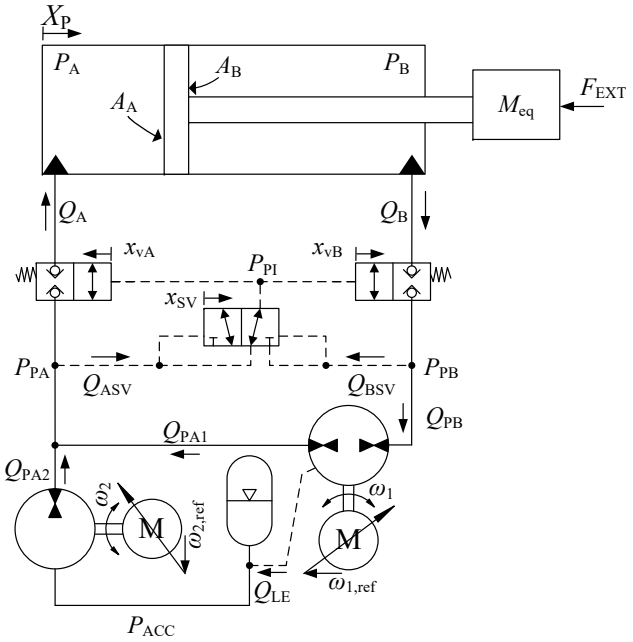

Figure 6: Asymmetric cylinder controlled by DvSP-system.

$$\ddot{X}_\mathrm{P} = \frac{A_\mathrm{A}(P_\mathrm{A} - \alpha P_\mathrm{B}) - \dot{X}_\mathrm{P} B_\mathrm{v} - F_C \tanh(\gamma \mathrm{sign}(\dot{X}_\mathrm{P})) - f(X_P, \dot{X}_P)}{M_\mathrm{eq}} \quad (1)$$

$$\dot{P}_\mathrm{A} = \frac{\beta_\mathrm{A}}{V_\mathrm{A}} \left(Q_\mathrm{A} - \dot{X}_\mathrm{P} A_\mathrm{A} \right) \quad (2)$$

$$\dot{P}_\mathrm{B} = \frac{\beta_\mathrm{B}}{V_\mathrm{B}} \left(\dot{X}_\mathrm{P} \alpha A_\mathrm{A} - Q_\mathrm{B} \right) \quad (3)$$

$$\dot{P}_\mathrm{PA} = \frac{\beta_\mathrm{PA}}{V_\mathrm{PA}} \left(Q_\mathrm{PA1} + Q_\mathrm{PA2} - Q_\mathrm{A} - Q_\mathrm{ASV} \right) \quad (4)$$

$$\dot{P}_\mathrm{PB} = \frac{\beta_\mathrm{PB}}{V_\mathrm{PB}} \left(Q_\mathrm{B} - Q_\mathrm{PB} - Q_\mathrm{BSV} \right) \quad (5)$$

$$\dot{P}_\mathrm{PI} = \frac{\beta_\mathrm{PI}}{V_\mathrm{PI}} \left(Q_\mathrm{ASV} + Q_\mathrm{BSV} \right) \quad (6)$$

$$\dot{P}_\mathrm{ACC} = \frac{Q_\mathrm{LE} - Q_\mathrm{PA2}}{\frac{V_\mathrm{ACC} + V_0 - V_\mathrm{g}}{\beta_\mathrm{ACC}} + \frac{V_\mathrm{g}}{\kappa P_\mathrm{ACC}}} \quad (7)$$

$$V_\mathrm{g} = \begin{cases} V_\mathrm{ACC} & p_\mathrm{ACC} < p_0 \\ V_\mathrm{ACC} \left(\frac{P_0}{P_\mathrm{ACC}} \right)^{\frac{1}{\kappa}} & p_\mathrm{ACC} > p_0 \end{cases} \quad (8)$$

$$Q_\mathrm{PA1} = \omega_1 D_1 - K_1(P_\mathrm{PA} - P_\mathrm{PB}) - K_1(P_\mathrm{PA} - P_\mathrm{ACC}) \quad (9)$$

$$Q_\mathrm{PB} = \omega_1 D_1 - K_1(P_\mathrm{PA} - P_\mathrm{PB}) + K_1(P_\mathrm{PB} - P_\mathrm{ACC}) \quad (10)$$

$$Q_\mathrm{PA2} = \omega_1 D_2 - K_2(P_\mathrm{PA} - P_\mathrm{ACC}) \quad (11)$$

$$Q_\mathrm{LE} = K_1(P_\mathrm{PA} - P_\mathrm{ACC}) + K_1(P_\mathrm{PB} - P_\mathrm{ACC}) \quad (12)$$

$$Q_{\mathrm{A}} = x_{\mathrm{vA}} K_{\mathrm{Qv}} \sqrt{|P_{\mathrm{PA}} - P_{\mathrm{A}}|}\ \mathrm{sign}(P_{\mathrm{PA}} - P_{\mathrm{A}}) \quad (13)$$

$$Q_{\mathrm{B}} = x_{\mathrm{vB}} K_{\mathrm{Qv}} \sqrt{|P_{\mathrm{B}} - P_{\mathrm{PB}}|}\ \mathrm{sign}(P_{\mathrm{B}} - P_{\mathrm{PB}}) \quad (14)$$

$$Q_{\mathrm{ASV}} = (1 - x_{\mathrm{sv}}) K_{\mathrm{Qsv}} \sqrt{|P_{\mathrm{PA}} - P_{\mathrm{PI}}|}\ \mathrm{sign}(P_{\mathrm{PA}} - P_{\mathrm{PI}}) \quad (15)$$

$$Q_{\mathrm{BSV}} = x_{\mathrm{sv}} K_{\mathrm{Qsv}} \sqrt{|P_{\mathrm{PB}} - P_{\mathrm{PI}}|}\ \mathrm{sign}(P_{\mathrm{PB}} - P_{\mathrm{PI}}) \quad (16)$$

$$\ddot{\omega}_1 = \omega_{\mathrm{n}}^2 \omega_{1,\mathrm{ref}} - 2\zeta\omega_{\mathrm{n}}\dot{\omega}_1 - \omega_{\mathrm{n}}^2\omega_1 \quad (17)$$

$$\ddot{\omega}_2 = \omega_{\mathrm{n}}^2 \omega_{2,\mathrm{ref}} - 2\zeta\omega_{\mathrm{n}}\dot{\omega}_2 - \omega_{\mathrm{n}}^2\omega_2 \quad (18)$$

$$x_{\mathrm{vA}} = x_{\mathrm{vB}} = \begin{cases} 0 & \text{for } P_{\mathrm{PI}} \le P_{\mathrm{CR}} \\ \frac{P_{\mathrm{PI}} - P_{\mathrm{CR}}}{P_{\mathrm{OP}} - P_{\mathrm{CR}}} & \text{for } P_{\mathrm{CR}} < P_{\mathrm{PI}} < P_{\mathrm{OP}} \\ 1 & \text{for } P_{\mathrm{PI}} \ge P_{\mathrm{OP}} \end{cases} \quad (19)$$

$$x_{\mathrm{sv}} = \begin{cases} 0 & \text{for } P_{\mathrm{PA}} < P_{\mathrm{PB}} \\ 0.5 & \text{for } P_{\mathrm{PA}} = P_{\mathrm{PB}} \\ 1 & \text{for } P_{\mathrm{PA}} > P_{\mathrm{PB}} \end{cases} \quad (20)$$

X_{P} is the cylinder piston position, F_C is a Coulomb friction constant, and γ is a switching parameter. B_{v} is a viscous friction coefficient and $f(X_P, \dot{X}_P)$ contains the gravitational load and the Coriolis force. P_{A}, P_{B}, P_{PA}, P_{PB}, P_{PI}, P_{ACC} are control volume pressures, V_g is the volume of the gas in the accumulator, Q_{PA1}, Q_{PB}, Q_{PA2} and Q_{LE} are pump flows modelled by the Wilson pump model using geometric pump displacements D_1, D_2 and laminar leakage coefficients K_1,K_2. Q_{A}, Q_{B}, Q_{ASV} and Q_{BSV} are valve flows modelled by the orifice equation, x_{vA}, x_{vB}, x_{sv} are valve poppet positions modelled as quasi static, i.e. no poppet/spool dynamics is included. P_{CR} and P_{OP} are valve cracking and full open pressures respectively. ω_1 and ω_2 are motor shaft speeds, ζ is damping ratio and ω_{n} is bandwidth used for modelling the dynamics of the electrical motor and drive. K_{Qv}, K_{Qsv} are valve flow gains and the motor shaft reference speeds $\omega_{1,\mathrm{ref}}$, $\omega_{2,\mathrm{ref}}$ are the two system inputs. Finally, the effective bulk modulus of the oil air mixture, β_i, $i = \{\mathrm{A,B,PA,PB,PI,ACC}\}$ is modelled being pressure dependent using, (Kim and Murrenhoff, 2012):

$$\beta_i(P_i) = \frac{(1-\epsilon)\left(1 + \frac{m(P_i - p_{\mathrm{atm}})}{\beta_{\mathrm{F}}}\right)^{-\frac{1}{m}} + \epsilon\left(\frac{p_{\mathrm{atm}}}{P_i}\right)^{\frac{1}{\kappa}}}{\frac{1-\epsilon}{\beta_{\mathrm{F}}}\left(1 + \frac{m(P_i - p_{\mathrm{atm}})}{\beta_{\mathrm{F}}}\right)^{-\frac{m+1}{m}} + \frac{\epsilon}{\kappa p_{\mathrm{atm}}}\left(\frac{p_{\mathrm{atm}}}{P_i}\right)^{\frac{\kappa+1}{\kappa}}}$$

where ϵ is the volumetric air content at atmospheric pressure (p_{atm}), β_F is the bulk modulus of the pure fluid, m is the pressure dependent bulk modulus gradient of the pure fluid and κ is the poly-tropic constant which is set to 1.4, assuming air to behave as an ideal gas and the compression process to be adiabatic. The effective bulk modulus is limited to 7500 bar, to include some mechanical compliance. All model parameters are listed on page 202.

5 Linear Models and Coupling Analysis

Two linear models are defined according to the two distinct operation modes, i.e. motion operation mode and load holding mode.
When deriving the linear models, M_{eq} and the accumulator pressure as well as the gravitational load and Coriolis force contained in $f(X_P, \dot{X}_P)$ are assumed constant close to the linearisation point. The bulk modulus are assumed equal and constant (β_0) in all control volumes. Similarly the volume of the cylinder chambers are assumed constant close to the linearisation point, and defined by $V_{\mathrm{A0}} = V_{\mathrm{A}}|_{\mathbf{x}_0}$, $V_{\mathrm{B0}} = V_{\mathrm{B}}|_{\mathbf{x}_0}$, $\rho = V_{\mathrm{B}}/V_{\mathrm{A}}$, $\rho_0 = V_{\mathrm{B0}}/V_{\mathrm{A0}}$, with $\mathbf{x}_0$ being the state vector at the linearisation point.

5.1 Motion Operation Mode

In motion operation mode the load holding valves LH_1 and LH_2 are considered ideal due to high flow gains for these valves in the fully open position, i.e. the pressures on each side of the valve are considered equal. Similarly the pressure dynamics in the pilot chamber is omitted, due to the small volume of this chamber relative to the remaining volumes in the system.

The simplified model structure, under the mentioned assumptions are illustrated in Fig. 7, with lowercase letters representing linear deviation variables.

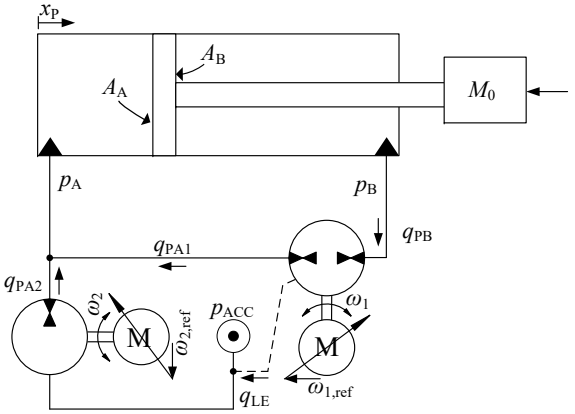

Figure 7: Simplified model structure for deriving linear model of the system in motion operating mode.

The linearised equations are given in Eq. (21) to (23):

$$\ddot{x}_{\mathrm{P}} = {M_{\mathrm{eq0}}}^{-1}\left(A_{\mathrm{A}}\left(p_{\mathrm{A}} - \alpha p_{\mathrm{B}}\right) - \dot{x}_{\mathrm{P}} B_{\mathrm{v}}\right) \quad (21)$$

$$\dot{p}_{\mathrm{A}} = \tfrac{\beta_0}{V_{\mathrm{A0}}}\left(\omega_1 D_1 + \omega_2 D_2 - (2K_1 + K_2)\, p_{\mathrm{A}} + K_1 p_{\mathrm{B}} - \dot{x} A_{\mathrm{A}}\right) \quad (22)$$

$$\dot{p}_{\mathrm{B}} = \tfrac{\beta_0}{\rho_0 V_{\mathrm{A0}}}\left(-\omega_1 D_1 - K_1\left(2p_{\mathrm{B}} - p_{\mathrm{A}}\right) + \dot{x} A_{\mathrm{A}}\right) \quad (23)$$

In state space form the dynamics may be represented as:

$$\dot{\mathbf{x}}_{\mathrm{M}} = \mathbf{A}_{\mathrm{M}}\mathbf{x}_{\mathrm{M}} + \mathbf{B}_{\mathrm{M}}\mathbf{u}_{\mathrm{M}}, \quad \mathbf{y}_{\mathrm{M}} = \mathbf{C}_{\mathrm{M}}\mathbf{x}_{\mathrm{M}} \tag{24}$$
$$\mathbf{x}_{\mathrm{M}} = [x_{\mathrm{P}} \;\; \dot{x}_{\mathrm{P}} \;\; p_{\mathrm{A}} \;\; p_{\mathrm{B}}]^T, \quad \mathbf{u}_{\mathrm{M}} = [\omega_1 \;\; \omega_2]^T$$

$$\mathbf{A}_{\mathrm{M}} = \begin{bmatrix} 0 & 1 & 0 & 0 \\ 0 & -\frac{B_{\mathrm{v}}}{M_{\mathrm{eq0}}} & \frac{A_{\mathrm{A}}}{M_{\mathrm{eq0}}} & -\frac{\alpha A_{\mathrm{A}}}{M_{\mathrm{eq0}}} \\ 0 & -\frac{\beta_0 A_{\mathrm{A}}}{V_{\mathrm{A0}}} & -\frac{\beta_0(2K_1+K_2)}{V_{\mathrm{A0}}} & \frac{\beta_0 K_1}{V_{\mathrm{A0}}} \\ 0 & \frac{\beta_0 \alpha A_{\mathrm{A}}}{\rho_0 V_{\mathrm{A0}}} & \frac{\beta_0 K_1}{\rho_0 V_{\mathrm{A0}}} & -2\frac{\beta_0 K_1}{\rho_0 V_{\mathrm{A0}}} \end{bmatrix}$$

$$\mathbf{B}_{\mathrm{M}} = \begin{bmatrix} 0 & 0 \\ 0 & 0 \\ \frac{\beta_0 D_1}{V_{\mathrm{A0}}} & \frac{\beta_0 D_2}{V_{\mathrm{A0}}} \\ \frac{-\beta_0 D_1}{\rho_0 V_{\mathrm{A0}}} & 0 \end{bmatrix} \quad \mathbf{C}_{\mathrm{M}} = \begin{bmatrix} 1 & 0 & 0 & 0 \\ 0 & 0 & 1 & 0 \\ 0 & 0 & 0 & 1 \end{bmatrix}$$

The subscript $_{\mathrm{M}}$ is used to denote motion operating mode.

5.2 Load Holding Mode

In load holding mode the load holding valves LH_1 and LH_2 are closed and assumed leakage free. Utilizing this assumption the simplified model structure is illustrated in Fig. 8, with lowercase letters representing linear deviation variables.

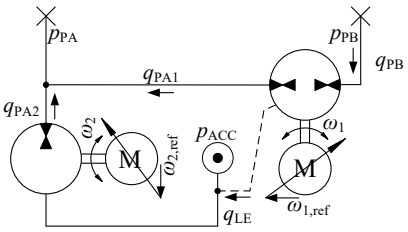

Figure 8: Simplified model system structure in load holding mode, used for deriving linearised model.

The linearised equations are given in Eq. (25) to (26), and represented in state space as:

$$\dot{p}_{\mathrm{PA}} = \tfrac{\beta_0}{V_{\mathrm{A0}}}\left(\omega_1 D_1 + \omega_2 D_2 - (2K_1 + K_2)\, p_{\mathrm{A}} + K_1 p_{\mathrm{B}}\right) \tag{25}$$

$$\dot{p}_{\mathrm{PB}} = \frac{\beta_0}{\rho_0 V_{\mathrm{A0}}}\left(-\omega_1 D_1 - K_1\left(2p_{\mathrm{B}} - p_{\mathrm{A}}\right)\right) \tag{26}$$

$$\dot{\mathbf{x}}_{\mathrm{LH}} = \mathbf{A}_{\mathrm{LH}}\mathbf{x}_{\mathrm{LH}} + \mathbf{B}_{\mathrm{LH}}\mathbf{u}_{\mathrm{LH}}, \quad \mathbf{y}_{\mathrm{LH}} = \mathbf{C}_{\mathrm{LH}}\mathbf{x}_{\mathrm{LH}} \tag{27}$$
$$\mathbf{x}_{\mathrm{LH}} = [p_{\mathrm{PA}} \;\; p_{\mathrm{PB}}]^T, \quad \mathbf{u}_{\mathrm{LH}} = [\omega_1 \;\; \omega_2]^T$$

$$\mathbf{A}_{\mathrm{LH}} = \begin{bmatrix} -\frac{\beta_0(2K_1+K_2)}{V_{\mathrm{A0}}} & \frac{\beta_0 K_1}{V_{\mathrm{A0}}} \\ \frac{\beta_0 K_1}{\rho_0 V_{\mathrm{A0}}} & -2\frac{\beta_0 K_1}{\rho_0 V_{\mathrm{A0}}} \end{bmatrix}$$

$$\mathbf{B}_{\mathrm{LH}} = \begin{bmatrix} \frac{\beta_0 D_1}{V_{\mathrm{A0}}} & \frac{\beta_0 D_2}{V_{\mathrm{A0}}} \\ \frac{-\beta_0 D_1}{\rho_0 V_{\mathrm{A0}}} & 0 \end{bmatrix} \quad \mathbf{C}_{\mathrm{M}} = \begin{bmatrix} 1 & 0 \\ 0 & 1 \end{bmatrix}$$

The subscript $_{\mathrm{LH}}$ is denoting load holding mode.

5.3 Electrical Motor Drive Model

The input to the linearised models are the shaft speeds (ω_1 and ω_2), thus the actuator dynamics has been neglected so far. To include these, a state space representation of the motor, motor drive and motor control dynamics is derived from Eq. (17) and (18):

$$\dot{\mathbf{x}}_{\mathrm{u}} = \mathbf{A}_{\mathrm{u}}\mathbf{x}_{\mathrm{u}} + \mathbf{B}_{\mathrm{u}}\mathbf{u}_{\mathrm{ref}}, \quad \mathbf{y}_{\mathrm{u}} = \mathbf{C}_{\mathrm{u}}\mathbf{x}_{\mathrm{u}} \tag{28}$$
$$\mathbf{x}_{\mathrm{u}} = [\omega_1 \;\; \omega_2]^T, \quad \mathbf{u}_{\mathrm{ref}} = [\omega_{1,\mathrm{ref}} \;\; \omega_{2,\mathrm{ref}}]^T$$
$$\mathbf{A}_{\mathrm{u}} = \begin{bmatrix} \mathbf{A}_{\mathrm{EM}} & \mathbf{0} \\ \mathbf{0} & \mathbf{A}_{\mathrm{EM}} \end{bmatrix} \quad \mathbf{A}_{\mathrm{EM}} = \begin{bmatrix} 0 & 1 \\ -\omega_{\mathrm{n}}^2 & -2\zeta\omega_{\mathrm{n}} \end{bmatrix}$$
$$\mathbf{B}_{\mathrm{u}} = \begin{bmatrix} 0 & 0 \\ \omega_{\mathrm{n}}^2 & 0 \\ 0 & 0 \\ 0 & \omega_{\mathrm{n}}^2 \end{bmatrix} \quad \mathbf{C}_{\mathrm{u}} = \begin{bmatrix} 1 & 0 & 0 & 0 \\ 0 & 0 & 1 & 0 \end{bmatrix}$$

5.4 Combined Linear Models

The linear models of the system in motion operating mode and load holding mode may be obtained by combining the respective models with the actuator models according to:

$$\dot{\mathbf{x}}_{\mathrm{cM}} = \mathbf{A}_{\mathrm{cM}}\mathbf{x}_{\mathrm{cM}} + \mathbf{B}_{\mathrm{cM}}\mathbf{u}_{\mathrm{ref}}, \quad \mathbf{y}_{\mathrm{M}} = \mathbf{C}_{\mathrm{cM}}\mathbf{x}_{\mathrm{cM}}$$
$$\mathbf{x}_{\mathrm{cM}} = \begin{bmatrix} \mathbf{x}_{\mathrm{M}} \\ \mathbf{x}_{\mathrm{u}} \end{bmatrix}, \quad \mathbf{A}_{\mathrm{cM}} = \begin{bmatrix} \mathbf{A}_{\mathrm{M}} & \mathbf{B}_{\mathrm{M}}\mathbf{C}_{\mathrm{u}} \\ \mathbf{0} & \mathbf{A}_{\mathrm{u}} \end{bmatrix}$$
$$\mathbf{B}_{\mathrm{cM}} = \begin{bmatrix} \mathbf{0} \\ \mathbf{B}_{\mathrm{u}} \end{bmatrix}, \quad \mathbf{C}_{\mathrm{cM}} = \begin{bmatrix} \mathbf{C}_{\mathrm{M}} & \mathbf{0} \end{bmatrix} \tag{29}$$
$$\dot{\mathbf{x}}_{\mathrm{cLH}} = \mathbf{A}_{\mathrm{cLH}}\mathbf{x}_{\mathrm{cLH}} + \mathbf{B}_{\mathrm{cLH}}\mathbf{u}_{\mathrm{ref}}, \quad \mathbf{y}_{\mathrm{LH}} = \mathbf{C}_{\mathrm{cLH}}\mathbf{x}_{\mathrm{cLH}}$$
$$\mathbf{x}_{\mathrm{cLH}} = \begin{bmatrix} \mathbf{x}_{\mathrm{LH}} \\ \mathbf{x}_{\mathrm{u}} \end{bmatrix}, \quad \mathbf{A}_{\mathrm{cLH}} = \begin{bmatrix} \mathbf{A}_{\mathrm{LH}} & \mathbf{B}_{\mathrm{LH}}\mathbf{C}_{\mathrm{u}} \\ \mathbf{0} & \mathbf{A}_{\mathrm{u}} \end{bmatrix}$$
$$\mathbf{B}_{\mathrm{cLH}} = \begin{bmatrix} \mathbf{0} \\ \mathbf{B}_{\mathrm{u}} \end{bmatrix}, \quad \mathbf{C}_{\mathrm{cLH}} = \begin{bmatrix} \mathbf{C}_{\mathrm{LH}} & \mathbf{0} \end{bmatrix} \tag{30}$$

The subscripts $_{\mathrm{cM}}$ and $_{\mathrm{cLH}}$ denote the combined linear models for motion operating mode and load holding mode respectively.

The combined linear models from Eq. (29) and (30) may be expressed by the transfer function matrices Eq. (31) and (32), (Philips and Parr, 2011):

$$\mathbf{y}_{\mathrm{M}}(s) = \mathbf{G}_{\mathrm{cM}}(s)\mathbf{u}_{\mathrm{ref}}(s)$$
$$\mathbf{G}_{\mathrm{cM}}(s) = \mathbf{C}_{\mathrm{cM}}(s\mathbf{I} - \mathbf{A}_{\mathrm{cM}})^{-1}\mathbf{B}_{\mathrm{cM}} \tag{31}$$
$$\mathbf{y}_{\mathrm{LH}}(s) = \mathbf{G}_{\mathrm{cLH}}(s)\mathbf{u}_{\mathrm{ref}}(s)$$
$$\mathbf{G}_{\mathrm{cLH}}(s) = \mathbf{C}_{\mathrm{cLH}}(s\mathbf{I} - \mathbf{A}_{\mathrm{cLH}})^{-1}\mathbf{B}_{\mathrm{cLH}} \tag{32}$$

5.5 Coupling Analysis

To analyse the degree of cross couplings or interactions in the system, the concept of the Relative Gain Array (RGA) is used (Glad and Ljung, 2000). In a multi-variable system the RGA-number may be used to analyse "how close" the system is to being a diagonal system, equivalently to indicate the severity of the off-diagonal elements (cross couplings). If a system is diagonal, a diagonal controller (decentralised control), may yield satisfying results. As such a RGA analysis is often utilised to select proper input/output pairings.

In motion operating mode, three system outputs $(x, p_{\mathrm{A}}, p_{\mathrm{B}})$ are present. It is not possible to control all three outputs independently, meaning that the cross couplings may be investigated for the following three 2×2 sub-matrices of $\mathbf{G}_{\mathrm{cM}}(s)$:

$$\mathbf{G}_{\mathrm{cM1}}(s) = \begin{bmatrix} G_{\omega_1 \to x} & G_{\omega_2 \to x} \\ G_{\omega_1 \to p_{\mathrm{A}}} & G_{\omega_2 \to p_{\mathrm{A}}} \end{bmatrix} \tag{33}$$

$$\mathbf{G}_{\mathrm{cM2}}(s) = \begin{bmatrix} G_{\omega_1 \to x} & G_{\omega_2 \to x} \\ G_{\omega_1 \to p_{\mathrm{B}}} & G_{\omega_2 \to p_{\mathrm{B}}} \end{bmatrix} \tag{34}$$

$$\mathbf{G}_{\mathrm{cM3}}(s) = \begin{bmatrix} G_{\omega_1 \to p_{\mathrm{A}}} & G_{\omega_2 \to p_{\mathrm{A}}} \\ G_{\omega_1 \to p_{\mathrm{B}}} & G_{\omega_2 \to p_{\mathrm{B}}} \end{bmatrix} \tag{35}$$

The transfer function matrix $G_{\mathrm{cLH}}(s)$ is a 2×2 matrix, meaning that only one input/output pairing must be investigated:

$$\mathbf{G}_{\mathrm{cLH}}(s) = \begin{bmatrix} G_{\omega_1 \to p_{\mathrm{PA}}} & G_{\omega_2 \to p_{\mathrm{PA}}} \\ G_{\omega_1 \to p_{\mathrm{PB}}} & G_{\omega_2 \to p_{\mathrm{PB}}} \end{bmatrix} \tag{36}$$

The Relative Gain Array number ($\mathrm{RGA}_{\#}$) is defined for diagonal input/output paring in Eq. (37) and off-diagonal pairing in Eq. (38), (Skogestad and Postlethwaite, 2005):

$$\mathrm{RGA}_{\#\mathrm{dia}} = \sum_{k,j} \Bigg| \underbrace{\mathbf{G}_i \times \left(\mathbf{G}_i^{-1}\right)^T}_{\text{RGA Elements}} - \begin{bmatrix} 1 & 0 \\ 0 & 1 \end{bmatrix} \Bigg| \tag{37}$$

$$\mathrm{RGA}_{\#\mathrm{off}} = \sum_{k,j} \Bigg| \underbrace{\mathbf{G}_i \times \left(\mathbf{G}_i^{-1}\right)^T}_{\text{RGA Elements}} - \begin{bmatrix} 0 & 1 \\ 1 & 0 \end{bmatrix} \Bigg| \tag{38}$$

where $i = \{\mathrm{cM}_1, \mathrm{cM}_2, \mathrm{cM}_3, \mathrm{cLH}\}$, and $\times$ here denotes element-by-element multiplication or Hadamard product. k, j is the number of row and columns in the transfer function matrix. For further details on the RGA and RGA-number the reader may consult Skogestad and Postlethwaite (2005) or Glad and Ljung (2000). Here it suffices to note that in case of ideal decoupling utilizing a diagonal input/output pairing the $\mathrm{RGA}_{\#\mathrm{dia}}$ and $\mathrm{RGA}_{\#\mathrm{off}}$ attain the values 0 and 4 respectively for all frequencies, while in case of ideal decoupling utilizing an off-diagonal input/output pairing the $\mathrm{RGA}_{\#\mathrm{dia}}$ and $\mathrm{RGA}_{\#\mathrm{off}}$ attain the values 4 and 0 respectively for all frequencies.

The evaluated RGA-numbers for load holding mode and motion operation mode are shown in Fig. 9 and 10. In load holding mode, both RGA-numbers are constantly equal to 2 in the considered frequency range. This means that a proper input/output pairing suited for a decentralised control strategy can not be identified. For motion operating mode, the three pairings in Fig. 10 are all seen to yield RGA-numbers highly above the desired values of 0 and 4 around 2 Hz, which is the eigenfrequency of the drive at this particular linearisation point. For frequencies below the eigenfrequency the RGA-numbers are closer to the desired values. As such the analysis suggests that if decentralised control strategy should be utilised, the closed loop bandwidths need to be well below the system eigenfrequency, and the input/output pairing should be made such that $\omega_{1,\mathrm{ref}}$ controls the piston position, while $\omega_{2,\mathrm{ref}}$ controls either chamber pressure A or B. However, because the RGA numbers are still rather far from the desired values of 0 and 4, it is found questionable whether using a decentralised control approach directly may yield satisfying results.

For both operation modes the coupling analysis reveals rather strong couplings which may render the performance using decentralised control unsatisfying. Therefore an alternative approach is desirable.

In Schmidt et al. (2017) a concept for decoupling the motion dynamics from the chamber pressure dynamics, by transforming the inputs and output states, are presented. For a pump-controlled system fundamentally different than the one proposed in the current paper, this is shown to effectively decouple the selected transformed/virtual states. As such a simple decentralised control structure may be used to control the transformed states, using conventional linear controllers. This strategy is adopted for the proposed system in the following section.

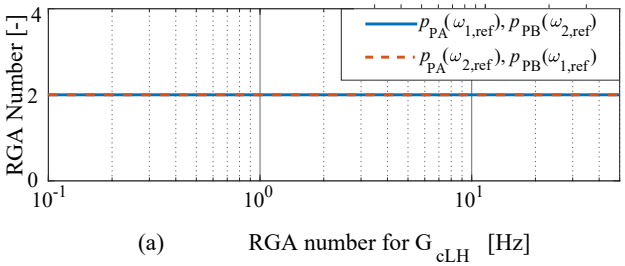

Figure 9: RGA numbers for diagonal and off-diagonal input/output pairings evaluated for the transfer function matrix $\mathbf{G}_{\mathrm{LH}}(s)$.

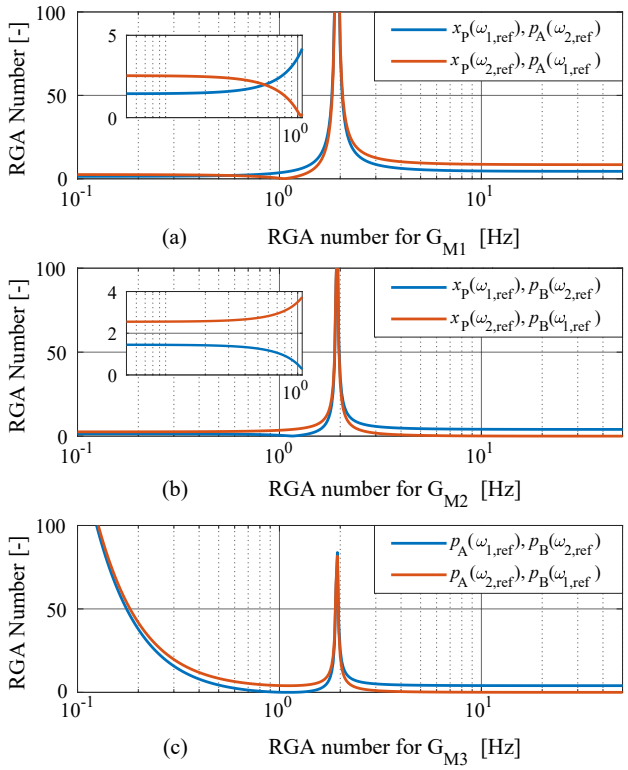

Figure 10: RGA numbers for diagonal and off-diagonal input/output pairings for $\mathbf{G}_{cM1}(s)$, $\mathbf{G}_{cM2}(s)$ and $\mathbf{G}_{cM3}(s)$.

6 Control Strategy

The overall control strategy is to derive a transformed system, where the evaluated RGA-numbers are significantly closer to the desired values of 0 and 4.

The physical input and output variables are transformed using the pre-compensator $\mathbf{W}_1$ and post-compensator $\mathbf{W}_2$ (Skogestad and Postlethwaite, 2005). Using these compensators or transformation matrices new virtual states may be defined as: $\tilde{\mathbf{y}} = \mathbf{W}_2\mathbf{y}$, $\tilde{\mathbf{u}} = \mathbf{W}_1^{-1}\mathbf{u}_{ref}$.

If defining $\mathbf{G}_M(s)$, $\mathbf{G}_{LH}(s)$ and $\mathbf{G}_u(s)$ to be the transfer function formulation of the dynamic systems represented by Eq. (24), (27) and (28), the following may be written (omitting (s) for brevity), for the system operating in motion mode:

$$\mathbf{u}_M = \mathbf{G}_u\mathbf{u}_{ref},\ \mathbf{u}_{ref} = \mathbf{W}_{1M}\tilde{\mathbf{u}}_M \ \Rightarrow\ \mathbf{u}_M = \mathbf{G}_u\mathbf{W}_{1M}\tilde{\mathbf{u}}_M \quad (39)$$

$$\tilde{\mathbf{y}}_M = \mathbf{W}_{2M}\mathbf{y}_M,\ \mathbf{y}_M = \mathbf{G}_M\mathbf{u}_M \ \Rightarrow\ \tilde{\mathbf{y}}_M = \mathbf{W}_{2M}\mathbf{G}_M\mathbf{u}_M \quad (40)$$

Substituting Eq. (39) into Eq. (40), gives the transformed system as:

$$\tilde{\mathbf{y}}_M = \mathbf{W}_{2M}\mathbf{G}_M\mathbf{G}_u\mathbf{W}_{1M}\tilde{\mathbf{u}}_M = \tilde{\mathbf{G}}_{cM}\tilde{\mathbf{u}}_M, \quad (41)$$

For load holding mode, the transformed system may be described in a similar manner as:

$$\tilde{\mathbf{y}}_{LH} = \mathbf{G}_{LH}\mathbf{G}_u\mathbf{W}_{1LH}\tilde{\mathbf{u}}_{LH} = \tilde{\mathbf{G}}_{cLH}\tilde{\mathbf{u}}_{LH}, \quad (42)$$

Please note, that for the transformed system operating in load holding mode, the output transformation matrix $\mathbf{W}_{2LH} = \mathbf{I}$.

The transformation matrices $\mathbf{W}_{1M}$, $\mathbf{W}_{2M}$ and $\mathbf{W}_{2LH}$ are chosen as static pre and post compensators. Due to the static gain of $\mathbf{G}_u$ being unity, $\mathbf{W}_{1M}$, $\mathbf{W}_{2M}$ and $\mathbf{W}_{2LH}$ may be designed by only considering $\mathbf{G}_M$ and $\mathbf{G}_{LH}$ respectively.

6.1 Transformed System in Motion Operation Mode

The task of deriving suitable transformation matrices $\mathbf{W}_{1M}$, $\mathbf{W}_{2M}$ and $\mathbf{W}_{2LH}$ are divided into subtasks. First the output transformation in motion operation mode, $\mathbf{W}_{2M}$, is derived.

6.1.1 Output Transformation

Instead of considering the physical pressure states, Schmidt et al. (2017) found it desirable to formulate an output transformation ($\mathbf{W}_{2LH}$) considering more *appropriate* pressure states. These appropriate states were selected to be the piston position, the virtual load pressure P_L, and the *level pressure* P_H:

$$P_L = P_A - \alpha P_B, \quad P_H = P_A + HP_B, \quad (43)$$

The load pressure is proportional to the piston force and as such closely related to the cylinder motion dynamics. The task is to define H, such that the virtual level pressure is decoupled from the piston motion/load pressure. By inserting the non-linear pressure dynamics from Eq. (2) to (5), and assuming $\beta = \beta_A = \beta_B$, the virtual pressure dynamics may be expressed as:

$$\begin{aligned}\dot{P}_L &= \dot{P}_A - \alpha\dot{P}_B \quad (44)\\ &= \tfrac{\beta}{\rho V_A}(\rho(Q_{PA1}+Q_{PA2}) + \alpha(Q_{PB} - A_A\dot{X}_P(\alpha^2+\rho))\\ \dot{P}_H &= \dot{P}_A + H\dot{P}_B + \dot{H}P_B \quad (45)\\ &= \tfrac{\beta}{\rho V_A}\left(\rho(Q_{PA1}+Q_{PA2}) - HQ_{PB} + \underbrace{A_A\dot{X}_P(\alpha H - \rho)}_{\Psi}\right)\\ &\quad + \frac{\dot{H}}{H+\alpha}(P_H - P_L)\end{aligned}$$

The assumption of equal bulk modulus in the two control volumes is justified in the fact, that in motion operation mode both chamber pressures are kept at an elevated level (e.g. 30 bar).

The term denoted Ψ in Eq. (45) represents a direct coupling between the piston velocity and the pressure gradient. To decouple the level pressure from the piston motion H is chosen as ρ/α, yielding $\Psi = 0$

The last term in Eq. (45) contains $\dot{H}$, which by the selection of H in fact creates another $\dot{X}_P$ dependent term. The derivative of H is given as:

$$\dot{H} = \frac{-\dot{X}_P A_A (\alpha + \rho)}{V_\mathrm{A} \alpha} \tag{46}$$

By the definition of H, the P_H dynamics is given by:

$$\begin{aligned}\dot{P}_H = &\frac{\beta}{\rho V_\mathrm{A}} (\rho(Q_{\mathrm{PA1}} + Q_{\mathrm{PA2}}) - H Q_{\mathrm{PB}}) \\ &- \dot{X}_\mathrm{P} \frac{A_\mathrm{A}}{V_\mathrm{A}} \frac{H+1}{H+\alpha}(P_H - P_\mathrm{L})\end{aligned} \tag{47}$$

Whether the last term in Eq. (47) yields severe cross coupling is not immediately evident. This has to be evaluated when the cross-couplings are analysed for the transformed system in section 6.3. For this purpose a linear representation of the transformed system is required.

The linear virtual pressure dynamics may be obtained by inserting the linearised pump flows and expressing ρ as a function of H and α:

$$\begin{aligned}\dot{p}_L = &\frac{\beta_0}{V_{A0} H_0} (\omega_1 D_1 (H_0 + 1) + \omega_2 D_2 H_0 \\ &- \dot{x}_\mathrm{P} A_A (H_0 + \alpha) - \frac{H_0}{H_0 + \alpha}(C_5 p_H - C_6 p_L)\Big)\end{aligned} \tag{48}$$

$$\begin{aligned}\dot{p}_H = &\frac{\beta_0}{V_{A0}} \Big(\omega_1 D_1 + \omega_2 D_2 - \frac{\omega_1 D_1}{\alpha} \\ &- \frac{(C_1 + C_2) p_H + (C_3 - C_2) p_L + C_4 \dot{x}_\mathrm{P}}{\alpha + H_0}\Big)\end{aligned} \tag{49}$$

$$C_1 = \left(2\alpha - 2 + \frac{2}{\alpha}\right) K_1 + \alpha K_2$$

$$C_2 = \frac{\dot{x}_{\mathrm{P}0} A_A (H_0 + 1)}{\beta}$$

$$C_3 = \left(2H_0 + 1 - \frac{H_0 + 2}{\alpha}\right) K_1 + H_0 K_2$$

$$C_4 = \frac{A_A (H_0 + 1)(p_{H0} - p_{L0})}{\beta}, \quad C_5 = -\frac{\alpha}{H_0} C_3$$

$$C_6 = \left(2H_0 + 2 + \frac{2}{H_0}\right) K_1 + H_0 K_2$$

The output transformation matrix $W_{2\mathrm{M}}$ may be established as:

$$\tilde{\mathbf{y}}_\mathrm{M} = \mathbf{W}_{\mathrm{M2}} \mathbf{y}_\mathrm{M}, \; \tilde{\mathbf{y}}_\mathrm{M} = \begin{bmatrix} x_\mathrm{P} \\ p_\mathrm{L} \\ p_H \end{bmatrix}, \mathbf{W}_{2\mathrm{M}} = \begin{bmatrix} 1 & 0 & 0 \\ 0 & 1 & -\alpha \\ 0 & 1 & H_0 \end{bmatrix}$$

6.1.2 Input Transformation

Virtual inputs, q_H q_L are defined such that the distribution of the motor speeds ω_1 and ω_2 is not directly present in the pressure dynamics. Based on the linear level and load pressure dynamics in Eq. (48) and Eq. (49):

$$q_L = \omega_1 D_1 (H_0 + 1) + \omega_2 D_2 H_0 \tag{50}$$

$$q_H = \omega_1 D_1 + \omega_2 D_2 - \frac{\omega_1 D_1}{\alpha} \tag{51}$$

This leads to the input transformation matrix, $\mathbf{W}_{1\mathrm{M}}$:

$$\tilde{\mathbf{u}}_\mathrm{M} = \mathbf{W}_{1\mathrm{M}}^{-1} \mathbf{u}_\mathrm{M}$$

$$\tilde{\mathbf{u}}_\mathrm{M} = [q_L \;\; q_H]^T, \; \mathbf{u}_\mathrm{M} = [\omega_1 \;\; \omega_2]^T$$

$$\mathbf{W}_{1\mathrm{M}}^{-1} = \begin{bmatrix} D_1 (H_0 + 1) & D_2 H_0 \\ (D_1 - \frac{D_1}{\alpha}) & D_2 \end{bmatrix}$$

$$\mathbf{W}_{1\mathrm{M}} = \begin{bmatrix} \frac{\alpha}{D_1 (H_0 + \alpha)} & -\frac{\alpha H_0}{D_1 (H_0 + \alpha)} \\ \frac{1-\alpha}{(H_0+\alpha) D_2} & \frac{H_0 \alpha + \alpha}{D_2 (H_0 + \alpha)} \end{bmatrix}$$

6.2 Transformed System in Load Holding Mode

In load holding mode only an input transformation matrix, $\mathbf{W}_{1\mathrm{LH}}$ is derived. This is done by defining virtual inputs directly from the linear pressure dynamics of p_{PA} and p_{PB} in Eq. (25) and (26), such that the distribution of the individual motor speeds is not present in the pressure dynamics:

$$q_\mathrm{A} = D_1 \omega_1 + D_2 \omega_2 \tag{52}$$

$$q_\mathrm{B} = -D_1 \omega_1 \tag{53}$$

$$\tilde{\mathbf{u}}_{\mathrm{LH}} = \mathbf{W}_{1\mathrm{LH}}^{-1} \mathbf{u}_{\mathrm{LH}}$$

$$\tilde{\mathbf{u}}_{\mathrm{LH}} = [q_\mathrm{A} \;\; q_\mathrm{B}]^T, \; \mathbf{u}_{\mathrm{LH}} = [\omega_1 \;\; \omega_2]^T$$

$$\mathbf{W}_{1\mathrm{LH}} = \begin{bmatrix} 0 & -\frac{1}{D_1} \\ \frac{1}{D_2} & \frac{1}{D_2} \end{bmatrix} \tag{54}$$

6.3 Coupling Analysis of Transformed Systems

To evaluate the cross couplings in the transformed systems, linear state space representations, without actuator dynamics may be established as:

$$\dot{\mathbf{x}}_{\mathrm{T,M}} = \mathbf{A}_{\mathrm{T,M}} \mathbf{x}_{\mathrm{T,M}} + \mathbf{B}_{\mathrm{T,M}} \mathbf{u}_{\mathrm{T,M}}, \quad \mathbf{y}_{\mathrm{T,M}} = \mathbf{C}_{\mathrm{T,M}} \mathbf{x}_{\mathrm{T,M}}$$

$$\mathbf{x}_{\mathrm{T,M}} = [x_\mathrm{P} \;\; \dot{x}_\mathrm{P} \;\; p_\mathrm{L} \;\; p_\mathrm{H}]^T, \quad \mathbf{u}_{\mathrm{T,M}} = [q_\mathrm{L} \;\; q_\mathrm{H}]^T$$

$$C_7 = \frac{\beta_0}{V_{\mathrm{A}0} (H_0 + \alpha)}$$

$$\mathbf{A}_{\mathrm{T,M}} = \begin{bmatrix} 0 & 1 & 0 & 0 \\ 0 & -\frac{B_\mathrm{v}}{M_{\mathrm{eq0}}} & \frac{A_\mathrm{A}}{M_{\mathrm{eq0}}} & 0 \\ 0 & -\frac{\beta_0 A_\mathrm{A}(H_0+\alpha)}{V_{\mathrm{A0}} H_0} & -C_6C_7 & C_5C_7 \\ 0 & -C_4C_7 & -(C_3-C_2)C_7 & -(C_1+C_2)C_7 \end{bmatrix}$$

$$\mathbf{B}_{\mathrm{T,M}} = \begin{bmatrix} 0 & 0 \\ 0 & 0 \\ \frac{\beta_0}{H_0 V_{\mathrm{A0}}} & 0 \\ 0 & \frac{\beta_0}{V_{\mathrm{A0}}} \end{bmatrix} \quad \mathbf{C}_{\mathrm{T,M}} = \begin{bmatrix} 1 & 0 & 0 & 0 \\ 0 & 0 & 0 & 1 \end{bmatrix}$$

The subscripts $_{\mathrm{T,M}}$ denote the transformed system in motion operating mode. From the above a 2×2 transfer function matrix may be derived, and used to evaluate cross couplings and for controller design.

The transformed system in load holding mode is denoted with the subscript $_{\mathrm{T,LH}}$, and is shown as a state space representation below:

$$\begin{aligned} \dot{\mathbf{x}}_{\mathrm{T,LH}} &= \mathbf{A}_{\mathrm{T,LH}}\mathbf{x}_{\mathrm{T,LH}} + \mathbf{B}_{\mathrm{T,LH}}\mathbf{u}_{\mathrm{T,LH}}, \\ \mathbf{y}_{\mathrm{T,LH}} &= \mathbf{C}_{\mathrm{T,LH}}\mathbf{x}_{\mathrm{T,LH}} \\ \mathbf{x}_{\mathrm{T,LH}} &= [p_{\mathrm{PA}} \quad p_{\mathrm{PB}}]^T, \quad \mathbf{u}_{\mathrm{T,LH}} = [q_{\mathrm{PA}} \quad q_{\mathrm{PB}}]^T \\ \mathbf{A}_{\mathrm{T,LH}} &= \begin{bmatrix} -\frac{\beta_0(2K_1+K_2)}{V_{\mathrm{A0}}} & \frac{\beta_0 K_1}{V_{\mathrm{A0}}} \\ \frac{\beta_0 K_1}{\rho_0 V_{\mathrm{A0}}} & -2\frac{\beta_0 K_1}{\rho_0 V_{\mathrm{A0}}} \end{bmatrix} \\ \mathbf{B}_{\mathrm{T,LH}} &= \begin{bmatrix} \frac{\beta_0}{V_{\mathrm{A0}}} & 0 \\ 0 & \frac{\beta_0}{H_0 \alpha V_{\mathrm{A0}}} \end{bmatrix} \quad \mathbf{C}_{\mathrm{T,LH}} = \begin{bmatrix} 1 & 0 \\ 0 & 1 \end{bmatrix} \end{aligned}$$

A 2×2 transfer function matrix may be derived to evaluate cross couplings and for control design purposes. By including the actuator dynamics (Eq. (28)),

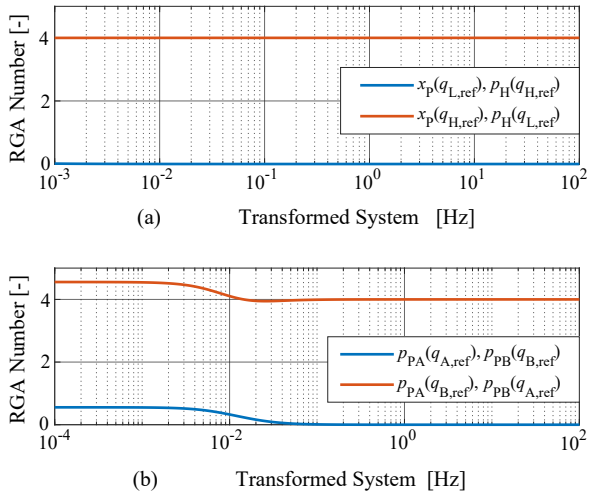

Figure 11: (a) RGA-numbers for the transformed system in motion operating mode. (b) RGA-numbers for the system operated in load holding mode.

the RGA numbers are evaluated for the transformed systems and shown in Fig. 11.

For the transformed system in motion operating mode a close to ideal decoupling in the entire frequency range may be observed. By varying the linearization point, and updating H accordingly, it is found that the RGA analysis yields results equivalent to the RGA-numbers shown in Fig. 11. This means that the proposed decoupling method, is independent of the operating point, if H is updated. The analysis shows that the transfer function matrix of the transformed system is close to diagonal, independently of operating point, and may thus be controlled by a diagonal controller (decentralised control), by neglecting the system cross-couplings (off-diagonal elements). The piston position is to be controlled by $q_{\mathrm{L,ref}}$ while p_{H} is paired with $q_{\mathrm{H,ref}}$.

For the transformed system in load holding mode, utilizing the input transformation matrix $\mathbf{W}_{1\mathrm{LH}}$, results in a significantly more decoupled system compared to the original system (Fig. 9). However, at low frequencies the RGA-numbers are not indicating an ideally decoupled system. All-together by Fig. 11b it is still easy to find that p_{PA} must be paired with $q_{\mathrm{A,ref}}$ and p_{PB} with $q_{\mathrm{B,ref}}$. For now this is done by accepting the minor cross couplings observed at low frequencies.

To sum up, it is assessed reasonable to control the transformed system in both motion operating mode and load holding mode using a decentralised control approach. The control strategy is summed up in Fig. 12. Note that H is updated during operation, to obtain proper decoupling as the cylinder moves (H changes). Also note that for the position control loop, velocity feedforward and pressure feedback have been included. The velocity feedforward gain is H dependent (see. section 7.2), effectively yielding a feedback of the piston position. The consequence of this may be included in a linear analysis similar to the one presented in section 6.

7 Controller Design

From Fig. 12 seven blocks need to be designed for the system to be operational. These include: level pressure reference generator, level pressure controller, pressure feedback filter, position controller, velocity feedforward gain, P_{PA} controller and finally P_{PB} controller.

Generally the controller design procedure is approached in a simple manner in this paper, as the main purpose is to illustrate the basic working principle of the drive, and the decoupling control strategy. The design procedure of the linear controllers follows the same pattern. First the most conservative design point is chosen by sweeping through different linearisation points and considering relative stability

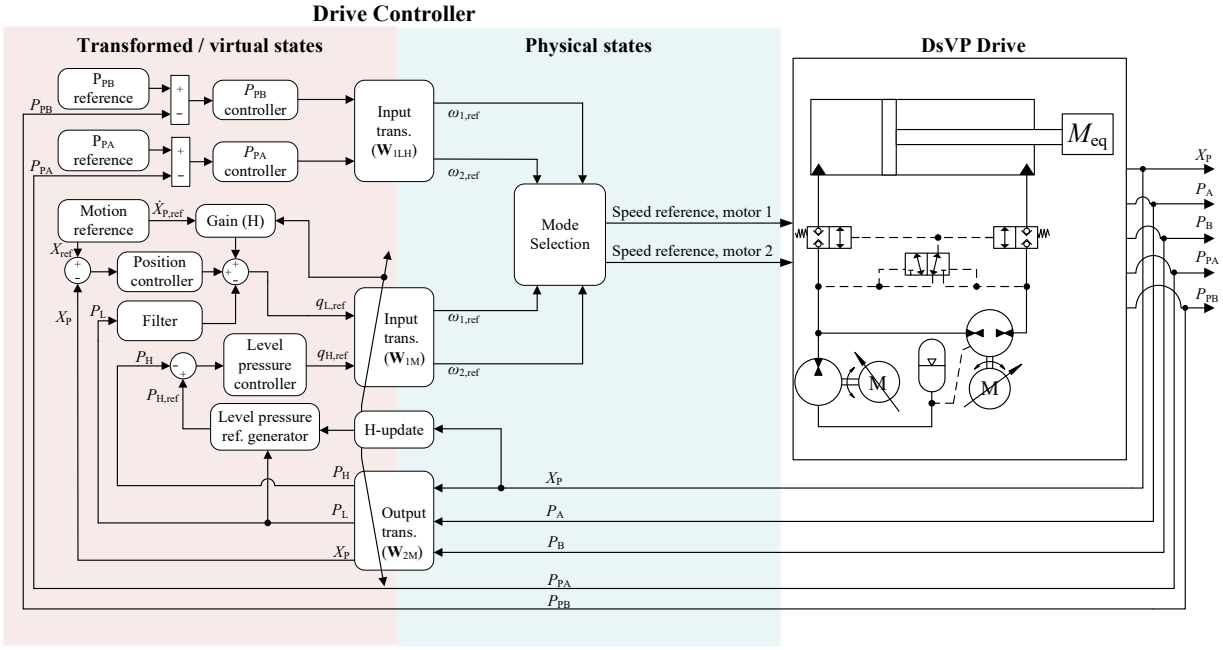

Figure 12: Schematic of the control structure for the proposed system.

margins. Even though this procedure ensures stability in the entire operating range, it may also yield unsatisfying performance due to large parameter variations (e.g. inertia) for the considered crane. For improved performance it may be beneficial to consider control structures, that include these parameters variations, such as gain scheduling or adaptive controllers. When a design point is chosen, linear controllers are designed based on desired stability margins.

7.1 Level Pressure Controller

The design of the level pressure controller is based on the transfer function $\frac{p_{\mathrm{H}}}{q_{\mathrm{H,ref}}}$, assuming that the cross coupling from $\frac{p_{\mathrm{H}}}{q_{\mathrm{L,ref}}}$ is negligible. The pressure in the low pressure chamber is defined as 30 bar, while the pressure in the load-carrying chamber is defined based on the crane load at a specific piston position.

By varying the piston position in the entire stroke length (0m to 2.8m) and the piston speed between minimum and maximum velocity (-45mm/s to 45 mm/s), the position of the open loop poles as a function of different linearisation points are found. This is illustrated in Fig. 13, where it is found that the placement of the pole close to origin is of special interest. It is found that the combination of large retraction velocities and small piston strokes yield this pole to be placed in the right half of the complex plane.

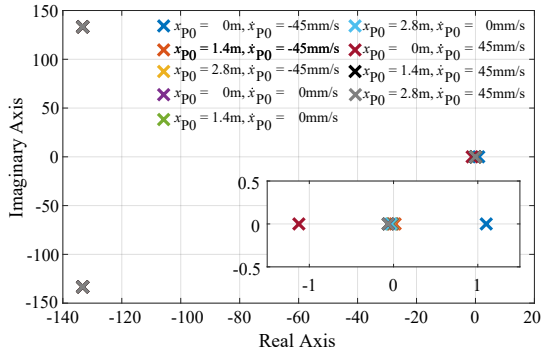

Figure 13: Variation of open loop poles for the transfer function $\frac{p_{\mathrm{H}}}{q_{\mathrm{H,ref}}}$.

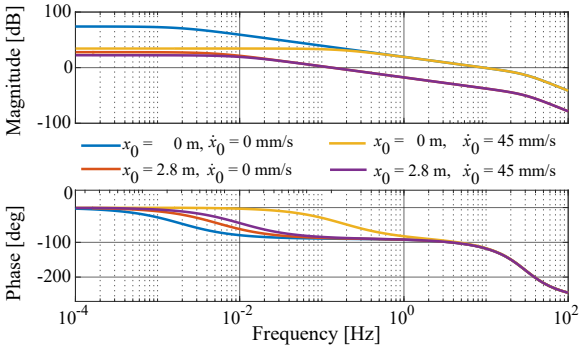

Figure 14: Open loop uncompensated Bode plot for $\frac{p_{\mathrm{H}}}{q_{\mathrm{H,ref}}}$.

By investigating the root locus of the system at 0m and -45 mm/s, it is evident that a P-controller is able to stabilize the closed loop system. Utilizing the Routh-Hurwitz stability criterion (Philips and Parr, 2011), it is found that the controller gain must be chosen between $0.02\ \frac{\mathrm{L}}{\mathrm{min\ Bar}} < K_p < 4.4 \frac{\mathrm{L}}{\mathrm{min\ Bar}}$.

To choose an appropriate controller gain within this range, the frequency response for different linearisation points (excluding those yielding a non-minimum phase system) are given in Fig. 14. The lowest relative stability margin is occurring at the fully retracted position, meaning that this is chosen as a conservative design point. A proportional gain of $K_P = 2.3\ \frac{\mathrm{L}}{\mathrm{min\ Bar}}$ is selected to yield a gain margin of 6 dB and a phase margin of 30 deg.

7.1.1 Level Pressure Reference Generator

The level pressure control loop controls a virtual pressure state. For this to be sensible also for the physical states, an appropriate level pressure reference must be generated. It is desired that neither P_{A} nor P_{B} decreases below a set pressure p_{set}, which is set to 30 bar. Which of the physical pressures P_{A} or P_{B} is to be controlled depends on the force working on the piston, i.e. the pressure in the load carrying-chamber should not be controlled directly. Therefore a load pressure dependent switching condition, $p_{\mathrm{L,s}}$, can be defined as the situation when both chamber pressures equal the set pressure, (Schmidt et al., 2017):

$$p_{\mathrm{A}} = p_{\mathrm{B}} = p_{\mathrm{set}} \quad \Rightarrow \quad p_{\mathrm{L,s}} = p_{\mathrm{set}}(1-\alpha) \tag{55}$$

Assuming the lower chamber pressure to equal p_{set} the chamber pressures may be described by:

$$p_{\mathrm{L}} > p_{\mathrm{L,s}} \quad \Rightarrow \quad p_{\mathrm{B}} = p_{\mathrm{set}}, p_{\mathrm{A}} = p_{\mathrm{L}} + \alpha p_{\mathrm{set}} \tag{56}$$

$$p_{\mathrm{L}} \leq p_{\mathrm{L,s}} \quad \Rightarrow \quad p_{\mathrm{A}} = p_{\mathrm{set}}, p_{\mathrm{B}} = \frac{p_{\mathrm{set}} - p_{\mathrm{L}}}{\alpha} \tag{57}$$

From the definition of p_{H} in Eq. (43) a load pressure reference may be calculated as:

$$p_{\mathrm{H,ref}} = \begin{cases} p_{\mathrm{L}} + (\alpha + H) p_{\mathrm{set}} & \text{for} \quad p_{\mathrm{L}} > p_{\mathrm{L,s}} \\ p_{\mathrm{set}} + H\left(\frac{p_{\mathrm{set}} - p_{\mathrm{L}}}{\alpha}\right) & \text{for} \quad p_{\mathrm{L}} \leq p_{\mathrm{L,s}} \end{cases} \tag{58}$$

The level pressure reference is thus a function of the load and set pressure as well as H. Examples of the load pressure reference values are shown in Fig. 15.

By controlling the pressure in the low pressure chamber using a virtual level pressure instead of the chamber pressure directly, it is not necessary to define which physical pressure to control. This is taken care of by the construction of the level pressure. This ensures smooth transition between operating quadrants (e.g direction of load force).

7.2 Motion Controller

The design of the motion controller is based on the transfer function $\frac{x}{q_{\mathrm{L,ref}}}$. Similarly to the design of the level pressure controller, the linearisation point is varied to identify a conservative design point, using the open loop frequency response. It is found that the influence of varying the piston speed is insignificant, meaning that it suffices to vary the piston position. In Fig. 16 the frequency responses at different piston positions are shown.

It is seen that the relative stability margins are smallest at the linearisation point, yielding the lowest eigenfrequency. Due to the increased inertia load for increasing piston position, the design point is selected at the fully extended position.

The system is observed to be poorly damped. To increase the damping of the system, the load pressure

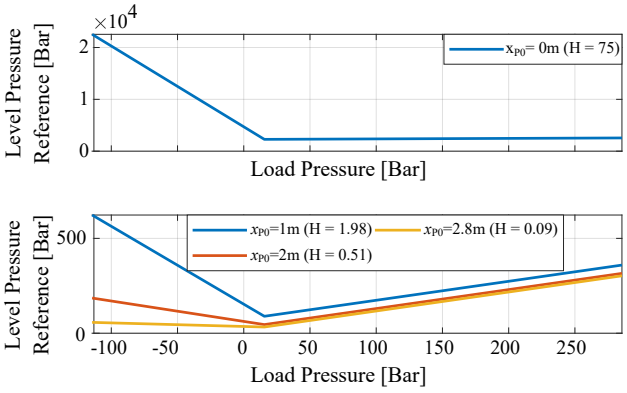

Figure 15: Examples of level pressure reference values as a function of load pressure evaluated using Eq. (58) for different piston positions.

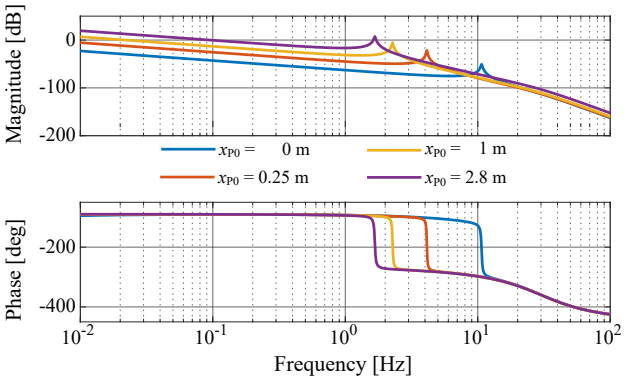

Figure 16: Open loop frequency response at different linearisation points for the transfer function $x_{\mathrm{p}}/q_{\mathrm{L,ref}}$. M_{eq} is included.

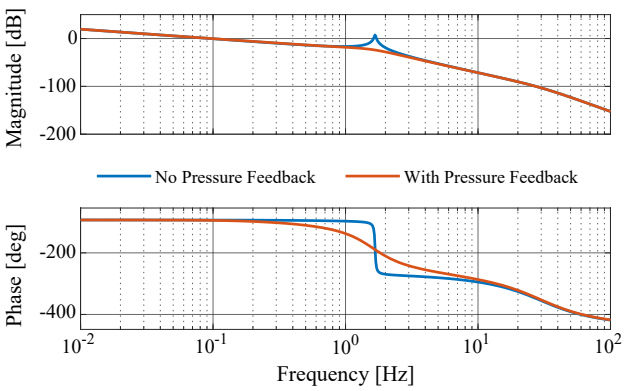

Figure 17: Comparison of frequency responses for the transfer function $x_{\mathrm{p}}/q_{\mathrm{L,ref}}$ (blue) and $x_{\mathrm{p}}/q^{\star}_{\mathrm{L,ref}}$(red).

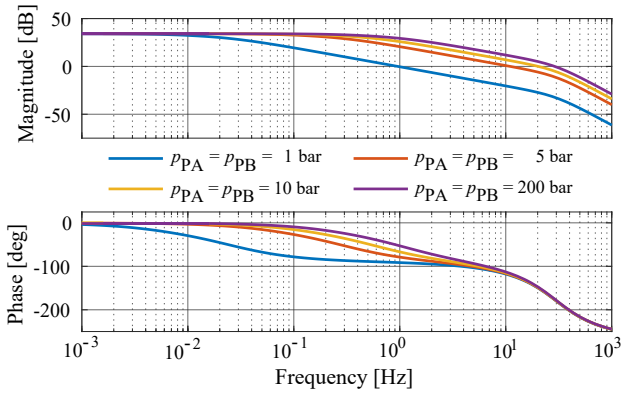

Figure 18: Open loop frequency responses for $\frac{p_{\mathrm{PA}}}{q_{\mathrm{A,ref}}}$ at different linearisation points.

is fed back through a high pass filter (Pedersen and Andersen, 2018):

$$q_{\mathrm{L,ref}} = q^{\star}_{\mathrm{L,ref}} - p_{\mathrm{L}} G_{\mathrm{c,PF}}(s) \tag{59}$$

$$G_{\mathrm{c,PF}}(s) = K_{\mathrm{PF}} \frac{s}{s + \omega_{\mathrm{PF}}} \tag{60}$$

The pole of the high pass filter, $G_{\mathrm{c,PF}}$, is placed one decade lower than the lowest system eigenfrequency and K_{PF} has been adjusted to yield a damping ratio of approximately 0.5. To avoid propagation of measurement noise, a low pass filter may be added in the pressure feedback path. The cut-off frequency of this filter, should be selected above the system eigenfrequency and below the frequency of the measurement noise. This is not considered in the current simulation study, as measurement noise has not been included. The effect of including the pressure feedback is clearly illustrated in Fig. 17, where the damping ratio of the system is seen to be significantly increased.

Based on the transfer function $\frac{x_{\mathrm{p}}}{q^{\star}_{\mathrm{L,ref}}}$, a PI controller has been designed to yield (minimum) relative stability margins of 6 dB and 45 deg for the considered conservative linearisation point:

$$G_{\mathrm{c,M}}(s) = \frac{K_{\mathrm{P}} s + K_{\mathrm{I}}}{s} \tag{61}$$

The controller coefficients are found to $K_{\mathrm{P}} = 6.3\ \frac{\mathrm{L}}{\mathrm{min\ mm}}$, $K_{\mathrm{I}} = 6.1\ \frac{\mathrm{L}}{\mathrm{min\ mm\ s}}$, placing the controller zero approximately one decade lower than the lowest system eigenfrequency.

To improve the position tracking ability, velocity feedforward as illustrated in Fig. 12 is implemented. The feedforward flow reference $q_{\mathrm{L,FF}}$, is calculated by combining Eq. (48) and (50) and setting the pressure gradient $\dot{p}_{\mathrm{L}} = 0$:

$$q_{\mathrm{L,FF}} = A_A(H + \alpha)\dot{X}_{\mathrm{P,ref}} \tag{62}$$

7.3 Pressure Controller

The pressure controllers when operating in load holding mode are chosen as PI controllers (Eq. (61)), because it is crucial that no steady state pressure error is present during transition between operation modes, to avoid load dropping.

The controllers are designed based on the transfer functions $\frac{p_{\mathrm{PA}}}{q_{\mathrm{A,ref}}}$ and $\frac{p_{\mathrm{PB}}}{q_{\mathrm{B,ref}}}$ respectively. In Fig. 18 the open loop frequency response for the former is shown at different linearisation points (varying line pressures). It is seen that the conservatively chosen design point must be selected as the linearisation point with the largest line pressures. The same may be shown for $\frac{p_{\mathrm{B}}}{q_{\mathrm{B,ref}}}$, which is left out for brevity.

Based on the transfer functions evaluated at the maximum allowed system pressure, PI controllers have been designed yielding stability margins of 8 dB and 40 deg for both pressure control loops.

8 Simulation Results

The performance of the proposed DvSP system and the derived control structure is evaluated by solving the non-linear dynamic equations from section 4 and the derived control structure. For this purpose a MatLAB/Simulink environment has been used in this study.

8.1 Motion Operating Mode

In Fig. 19 the performance of the system performing the motion trajectory in section 3 is presented. Note

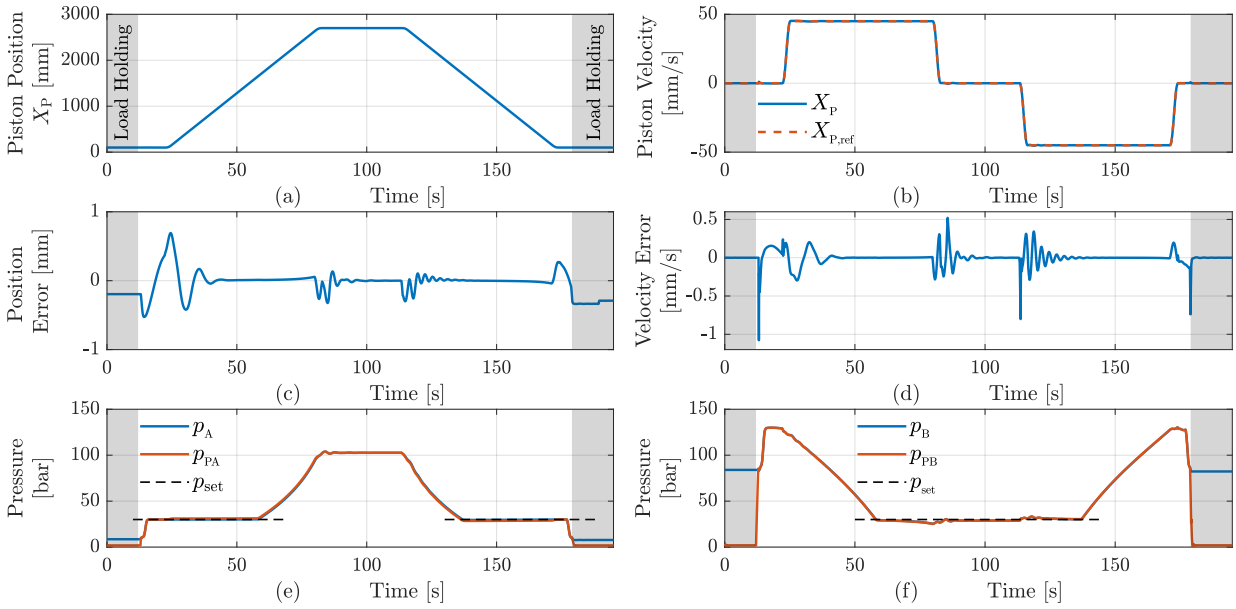

Figure 19: Performance of the proposed DvSP system performing the trajectory presented in section 3. The grey areas indicate that the system is operated in load holding mode, while being controlled in motion operation mode between these. (a) Piston position; (b) Piston velocity and reference; (c) Piston position error; (d) Piston velocity error; (e) Pressure in the piston chamber and adjacent transmission line; (f) Pressure in the rod chamber and adjacent transmission line.

that in the first and last approximately 20 s in Fig. 19 (grey areas), the system is controlled in load holding mode, while it is controlled in motion operating between these.

In Fig. 19a to Fig. 19d the motion tracking performance is visualised. Generally, rather accurate motion tracking is present in the entire trajectory, where the maximum position error is kept well within ±1mm. The largest position/velocity errors are present during the acceleration phase, where low frequency and amplitude velocity oscillations are also seen to be present. These oscillations are found to originate from a swinging payload. The oscillations are suppressed at a slow rate (≈20s), meaning that a room for improvement in terms of re-designing the active oscillation damping is present.

Regarding the level pressure control, it is found that the low pressure chamber is successfully controlled to the vicinity of the set pressure (30 bar). Deviations of a few bar from the set pressure is observed, especially as the piston position is increased. This is related to the conservative controller design approach leading to the level pressure being designed for the fully retracted position. The level pressure control is of secondary importance compared to the motion performance and therefore the small pressure deviations are not a concern. Most importantly, the level pressure control ensures that the load holding valves remains fully open as desired. Also note that even at full speed the differences between pressures P_A, P_{PA} and P_B, P_{PB} respectively are small, i.e. the pressure drops across the load holding valves in the fully open position are small. This is essential for energy-efficient operation.

A last thing to note from Fig. 19 is that the concept of controlling the level pressure, yields a smooth transition between operation quadrants.

8.2 Load Holding Mode and Mode Transition

In load holding mode two important operations are required:

1. Elevate the transmission line pressures to equal the chamber pressures during transition between load holding mode and mode operation mode. This is needed to avoid load drop and non smooth transition.

2. Reduce energy consumption when load is stationary.

Fig. 20 is a zoomed-in version of Fig. 19, where the transition between the two operation modes is highlighted.

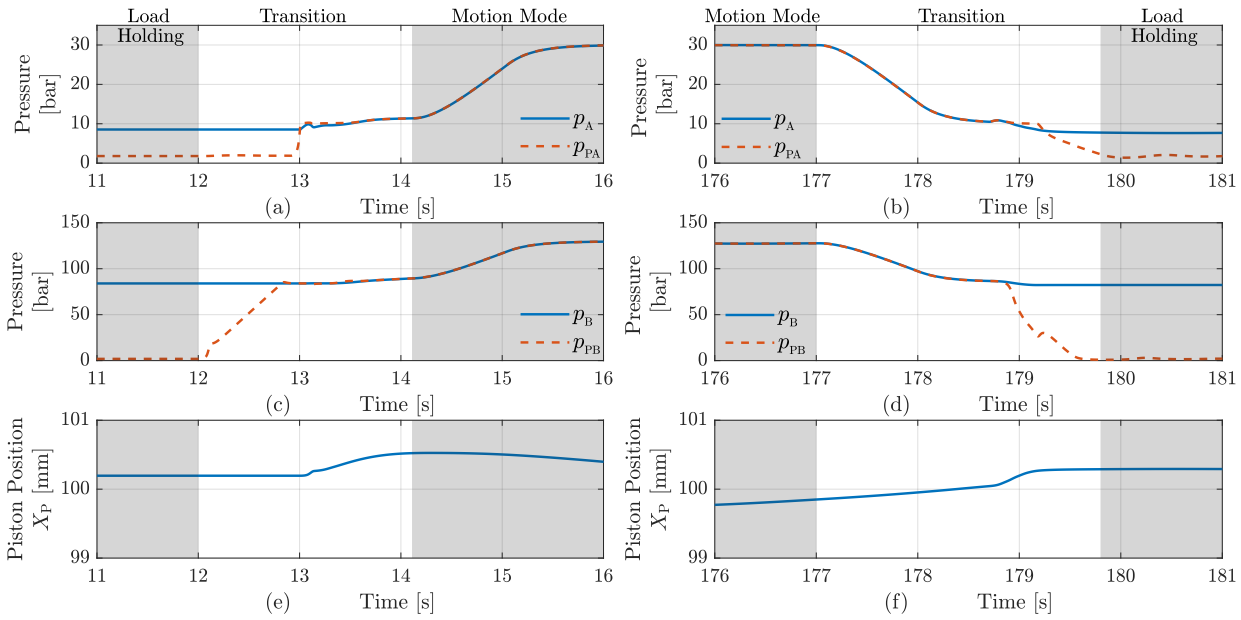

Figure 20: Transition between operation modes. (a) P_A and P_{PA} in transition between load holding and motion operating mode; (b) P_A and P_{PA} in transition between motion operating and load holding mode; (c) P_B and P_{PB} in transition between load holding and motion operating mode; (d) P_B and P_{PB} in transition between motion operating and load holding mode; (e) Piston position in transition between load holding and motion operating mode; (f) Piston position in transition between motion operating and load holding mode.

In Fig. 20a, 20c and 20e the focus is on the transition between load holding mode to motion operation mode. During transition (from 12 s to 14 s), the pressure in the transmission line adjacent to the load-carrying chamber, in this case P_{PB}, is controlled to equal the pressure in the cylinder chamber, P_B. The load holding valves are still fully closed. When P_{PB} has settled at P_B, P_A is increased in order to open the load holding valves. When the pressures P_A and P_{PA} are slightly larger than the cracking pressure (≈ 1 bar) of the load holding valves, the operating mode is changed to motion mode. In motion mode the lowest chamber pressure is further increased, to a value well above the full open pressure of the load holding valves. In Fig. 20e it may be seen that the piston position is steady until the lowest pressure has reached the cracking pressure of the load holding valve. During the transition period, the piston position is uncontrolled, leading to a slight drift in piston position. This is corrected as the system enters motion operation mode.

In Fig. 20b, 20d and 20f the focus is on the transition between motion operating mode and load holding mode. In the transition period (177s to 180 s) the pressure in the low pressure chamber is reduced to the cracking pressure of the load holding valves. When this pressure is reached, the system is operated in load holding mode and the transmission lines pressures are actively controlled to equal the accumulator pressure in order to reduce the energy consumption. In Fig. 20f it is observed that during the transition period, the piston position drifts approximately 0.5 mm. Because the cylinder is locked in load holding mode, this cannot be corrected. The position drift of 0.5 mm results in

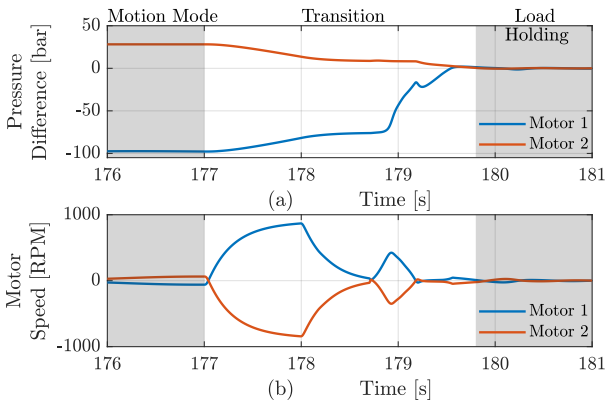

Figure 21: (a) Pressure difference across pumps during mode transition and in load holding mode. (b) Shaft speeds during mode transition and in load holding mode.

a movement of up 5.2 mm of the tool-center, for the crane considered in this investigation. To reduce this, further investigation into handling this mode transition is needed.

The active utilization of the load holding mode to decrease energy consumption, i.e. the load holding valves are not only a safety measure, requires that the pump torque is reduced in load holding mode. This is done by setting the reference pressures for the transmission line control to equal the current accumulator pressure. As illustrated by Fig. 21, this reduces the pressure difference across both pumps to ≈ 0 bar, reducing shaft torques, in turn reducing current losses in the motor. From Fig. 21 the shaft speed is seen to decrease to 0 RPM, when the load is carried by the load holding valves, reducing the shaft power to 0 W.

9 Conclusion

In this paper a self-contained pump-controlled cylinder drive with a pressure controlled hydraulic lock is proposed. A simple hydraulic architecture based on two variable-speed electrical motors each connected to a fixed-displacement hydraulic pump, with an innovative load holding sub-circuit is presented. The functionality of the load holding sub-circuit requires that the lowest cylinder chamber pressure is controlled accurately, without affecting the motion performance of the cylinder piston, which is found non-trivial due to severe cross couplings in the system. Therefore a control strategy aiming on state decoupling is derived based on input/output transformations. An analysis shows that the cross couplings in the transformed system are significantly decreased, and a simple decentralised control strategy is adopted for controlling the transformed system. Simulation results confirm the applicability of the drive architecture and the proposed decoupling strategy. Good position tracking performance and pressure control as well as smooth transition between operation quadrants are demonstrated. Furthermore, a close to bump-less transition between load holding and motion mode are seen, showing that a potential for utilising the load holding functionality actively to reduce energy consumption when the load is to be kept stationary, is present. The simulation results suggest a potential for future load carrying applications to be based on the proposed concept.

Acknowledgments

The research in this paper has received funding from The Research Council of Norway, SFI Offshore Mechatronics, project number 237896/O30.

Key Parameter List

	Description	Value
α	Cylinder area ratio	0.48 [-]
β_F	Bulk modulus of pure fluid	15000 bar
ϵ	Volumetric air content in oil	0.75 %
γ	Switching parameter	5000 [-]
κ	Poly-tropic constant	1.4 [-]
ω_n	Bandwidth, el. motor	30 Hz
ζ	Damping ratio, el. motor	0.7 [-]
$\mathrm{A_A}$	Piston Area	491 $\mathrm{cm^2}$
$\mathrm{A_B}$	Rod Area	236 $\mathrm{cm^2}$
B_v	Viscous friction constant	40000 $\frac{\mathrm{Ns}}{\mathrm{m}}$
D_1	Geometric displacement	26 $\frac{\mathrm{cm^3}}{\mathrm{rev}}$
D_2	Geometric displacement	28 $\frac{\mathrm{cm^3}}{\mathrm{rev}}$
F_C	Coulomb friction constant	5000 N
K_1	Leakage coefficient, pump 1	5.4 $\frac{\mathrm{mL}}{\mathrm{minbar}}$
K_2	Leakage coefficient, pump 2	11.4 $\frac{\mathrm{mL}}{\mathrm{minbar}}$
K_{Qv}	Flow gain, $\mathrm{LH_1}$ and $\mathrm{LH_2}$	127 $\frac{\mathrm{L}}{\mathrm{min}\sqrt{\mathrm{bar}}}$
K_{Qsv}	Flow gain, shuttle valve	0.3 $\frac{\mathrm{L}}{\mathrm{min}\sqrt{\mathrm{bar}}}$
m	Bulk modulus gradient	11.4 [-]
P_0	Accumulator precharge pres.	1.1 bar
P_{CR}	Cracking pressure	10 bar
P_{OP}	Full open pressure	20 bar
$\mathrm{V_{0A}}$	Initial volume	2.0 L
$\mathrm{V_{0B}}$	Initial volume	72.3 L
$\mathrm{V_{PA}}$	Line PA-volume	0.5 L
$\mathrm{V_{PB}}$	Line PB-volume	0.5 L
$\mathrm{V_{PI}}$	Pilot Line volume	0.1 L
$\mathrm{V_{ACC}}$	Accumulator volume	288.0 L
$\mathrm{V_0}$	Accumulator line volume	1.0 L

References

Brahmer, B. CLDP - Hybrid Drive using Servo Pump in Closed Loop. In *Proceedings of the 8th International Fluid Power Conference, Dresden, Germany, March 26-28*. pages 93–102, 2012.

Çalkan, H., Balkan, T., and Platin, B. E. A Complete Analysis and a Novel Solution for Instability in Pump Controlled Asymmetric Actuators. *Journal of Dynamic Systems, Measurement, and Control*, 2015. 137(9). doi:10.1115/1.4030544.

Costa, G. K. and Sepehri, N. Four-Quadrant Analysis and System Design for Single-Rod Hydrostatic Actuators. *Journal of Dynamic Systems, Measurement, and Control*, 2018. 141(2). doi:10.1115/1.4041382.

Dantlgraber, J. Hydraulic System for a Differential Piston Type Cylinder. 1993. URL https://patentimages.storage.googleapis.com/b1/da/49/ce4d84ab1ec11c/US5179836.pdf. United States Patent, Patent Number: 5179836, Company: Mannesmann Rexroth GmbH.

Donkov, V., Andersen, T. O., and Pedersen, H. C. Applying Digital Hydraulic Technology on a Knuckle Boom Crane Applying Digital Hydraulic Technology on a Knuckle Boom Crane. *The Ninth Workshop on Digital Fluid Power, September 7-8, 2017, Aalborg, Denmark*, 2017.

Donkov, V. H., Andersen, T. O., Pedersen, H. C., and Ebbesen, M. K. Application of Model Predictive Control in Discrete Displacement Cylinders to Drive a Knuckle Boom Crane. *Global Fluid Power Society PhD Symposium*, 2018. doi:10.1109/GFPS.2018.8472363.

Feuser, A., Dantlgraber, J., Spath, D., and Wilke, O. Servopumpeantriebe für Differentialzylinder. *Ölhydraulik und Pneumatik*, 1995. 39:540–544.

Glad, T. and Ljung, L. *Control Theory - Multivariable and Nonlinear Methods*. Taylor & Francis, 2000.

Gøytil, P., Padovani, D., and Hansen, M. R. On the Energy Efficiency of Dual Prime Mover Pump-Controlled Hydraulic Cylinders. In *Proceedings of the ASME/BATH 2019 Symposium on Fluid Power and Motion Control, Sarasota, Florida, USA, October 7-9*. 2019.

Gøytil, P. H., Padovani, D., and Hansen, M. R. A novel solution for the elimination of mode switching in pump-controlled single-rod cylinders. *Actuators*, 2020. 9(1). doi:10.3390/act9010020.

Grønkær, N., Hansen, K. V., Johansen, P., and Schmidt, L. Tribotronics in Electro-Hydraulic Actuator Technology: Improving Durability by Control. In *Proceedings of ASME/BATH 2020 Symposium on Fluid Power and Motion Control*. pages 1–9, 2020.

Hagen, D., Padovani, D., and Ebbesen, M. K. Study of a Self-Contained Electro-Hydraulic Cylinder Drive. *Global Fluid Power Society PhD Symposium*, 2018. pages 1–7. doi:10.1109/GFPS.2018.8472360.

Hagen, D., Pawlus, W., Ebbesen, M. K., and Andersen, T. O. Feasibility Study of Electromechanical Cylinder Drivetrain for Offshore Mechatronic Systems. *Modeling, Identification and Control: A Norwegian Research Bulletin*, 2017. 38(2):59–77. URL http://www.mic-journal.no/ABS/MIC-2017-2-2.asp, doi:10.4173/mic.2017.2.2.

Hedegaard Hansen, A., F Asmussen, M., and Bech, M. M. Energy optimal tracking control with discrete fluid power systems using model predictive control. In *Proceedings of the Ninth Workshop on Digital Fluid Power, Aalborg, Denmark, September 7-8*. 2017.

Hedegaard Hansen, A., F Asmussen, M., and Bech, M. M. Model Predictive Control of a Wave Energy Converter with Discrete Fluid Power Power Take-Off System. *Energies*, 2018. 11(3):635. doi:10.3390/en11030635.

Hedegaard Hansen, A. and Pedersen, H. C. Optimal configuration of a discrete fluid power force system utilised in the PTO for WECs. *Ocean Engineering*, 2016. 117:88–98. doi:10.1016/j.oceaneng.2016.03.032.

Helduser, S. Electric-hydrostatic drivean innovative energy-saving power and motion control system. *Proceedings of the Institution of Mechanical Engineers, Part I: Journal of Systems and Control Engineering*, 1999. 213(5):427–437. URL http://journals.sagepub.com/doi/10.1243/0959651991540250, doi:10.1243/0959651991540250.

Hewett, A. J. Hydraulic Circuit Flow Control. 1994. United States Patent, Patent Number: 5329767.

Imam, A., Rafiq, M., Jalayeri, E., and Sepehri, N. Design, Implementation and Evaluation of a Pump-Controlled Circuit for Single Rod Actuators. *Actuators*, 2017. 6. doi:10.3390/act6010010.

Jalayeri, E., Imam, A., Tomas, Z., and Sepehri, N. A throttle-less single-rod hydraulic cylinder positioning system: Design and experimental evaluation. *Advances in Mechanical Engineering*, 2015. 7(5). doi:10.1177/1687814015583249.

Ketelsen, S., Andersen, T. O., Ebbesen, M. K., and Schmidt, L. Mass Estimation of Self-contained Linear Electro-Hydraulic Actuators and Evaluation of the Influence on Payload Capacity of a Knuckle Boom Crane. In *Proceedings of the ASME/BATH 2019 Symposium on Fluid Power and Motion Control, Sarasota, Florida, USA, October 7-9*. 2019a.

Ketelsen, S., Kolks, G., Andersen, T. O., Schmidt, L., and Weber, J. Bootstrap Reservoir Concepts for Electro-hydraulic Compact Cylinder Drives. In *Proceedings of the 12th International Fluid Power Conference*. 2020a.

Ketelsen, S., Padovani, D., Andersen, T., Ebbesen, M., and Schmidt, L. Classification and Review of Pump-Controlled Differential Cylinder Drives. *Energies*, 2019b. 12(7):1293. doi:10.3390/en12071293.

Ketelsen, S., Padovani, D., Ebbesen, M. K., Andersen, T. O., and Schmidt, L. A Gasless Reservoir Solution for Electro-Hydraulic Compact Drives with Two Prime Movers. In *Proceedings of ASME/BATH 2020 Symposium on Fluid Power and Motion Control*. 2020b.

Ketelsen, S., Schmidt, L., Donkov, V. H., and Andersen, T. O. Energy Saving Potential in Knuckle Boom Cranes using a Novel Pump Controlled Cylinder Drive. *Modeling, Identification and Control*, 2018. 39(2):73–89. doi:10.4173/mic.2018.2.3.

Kim, S. and Murrenhoff, H. Measurement of Effective Bulk Modulus for Hydraulic Oil at Low Pressure. *Journal of Fluids Engineering*, 2012. 134(2):021201. doi:10.1115/1.4005672.

Linjama, M., Laamanen, A., and Vilenius, M. Is it Time for Digital Hydraulics? *Proceedings of the 8th Scandinavian International Conference on Fluid Power, SICFP, Vol1*, 2003. (March):347–366.

Lodewyks, J. *Der Differentialzylinder im geschlossenen hydrostatischen Kreislauf*. Ph.D. thesis, RWTH Aachen, 1994.

Michel, S. and Weber, J. Energy-efficient electrohydraulic compact drives for low power applications. In *Proceedings of the ASME/BATH 2012 Fluid Power and Motion Control, Bath, United Kingdom, September 12-14*. pages 93–107, 2012.

Minav, T., Bonato, C., Sainio, P., and Pietola, M. Direct Driven Hydraulic Drive. In *Proceedings of the 9th International Fluid Power Conference, Aachen, Germany, March 24-26*. pages 7–11, 2014.

Neubert, T. *Untersuchungen von drehveränderbaren Pumpen*. Ph.D. thesis, TU Dresden, 2002.

Padovani, D., Ketelsen, S., Hagen, D., and Schmidt, L. A Self-Contained Electro-Hydraulic Cylinder with Passive Load-Holding Capability. *Energies*, 2019. 12(2):292. doi:10.3390/en12020292.

Padovani, D., Ketelsen, S., and Schmidt, L. Downsizing the Electric Motors of Energy Efficient Self-Contained Electro-hydraulic Systems by Hybrid Technologies. In *Proceedings of the ASME/BATH Symposium on Fluid Power and Motion Control*. pages 1–10, 2020.

Pedersen, H. C. and Andersen, T. O. Pressure Feedback in Fluid Power Systems - Active Damping Explained and Exemplified. *IEEE Transactions on Control Systems Technology*, 2018. 26(1):102–113. doi:10.1109/TCST.2017.2650680.

Pedersen, H. C., Schmidt, L., Andersen, T. O., and H. Brask, M. Investigation of New Servo Drive Concept Utilizing Two Fixed Displacement Units. *JFPS International Journal of Fluid Power System*, 2014. 8(1):1–9. doi:10.5739/jfpsij.8.1.

Philips, C. and Parr, J. *Feedback Control Systems, 5th Edition*. Pearson, fifth edit edition, 2011. ISBN: 978-93-325-0760-9.

Quan, Z., Quan, L., and Zhang, J. Review of energy efficient direct pump controlled cylinder electro-hydraulic technology. *Renewable and Sustainable Energy Reviews*, 2014. 35:336–346. doi:10.1016/j.rser.2014.04.036.

Rahmfeld, R. and Ivantysynova, M. Displacement controlled linear actuator with differential cylinder - A way to save primary energy in mobile machines. In *Proceedings of the 5th International Conference on Fluid Power Transmission and Control, Hangzhou, China, April 4-5*. 2001.

Schmidt, L., Groenkjaer, M., Pedersen, H. C., and Andersen, T. O. Position Control of an OverActuated Direct Hydraulic Cylinder Drive. *Control Engineering Practice*, 2017. 64:1–14. doi:10.1016/J.CONENGPRAC.2017.04.003.

Schmidt, L., Ketelsen, S., Brask, M. H., and Mortensen, K. A. A Class of Energy Efficient Self-Contained Electro-Hydraulic Drives with Self-Locking Capability. *Energies*, 2019a. 12(10):1866. doi:10.3390/en12101866.

Schmidt, L., Ketelsen, S., Grønkær, N., and Hansen, K. V. On Secondary Control Principles in Pump Controlled Electro-Hydraulic Linear Actuators. In *Proceedings of ASME/BATH 2020 Symposium on Fluid Power and Motion Control*. pages 1–13, 2020.

Schmidt, L., Ketelsen, S., Padovani, D., and Mortensen, K. A. Improving the Efficiency and Dynamic Properties of a Flow Control Unit in a Self-Locking Compact Electro-Hydraulic Cylinder Drive.

In *Proceedings of the ASME/BATH 2019 Symposium on Fluid Power and Motion Control, Sarasota, Florida, USA, October 7-9*. 2019b.

Schmidt, L., Roemer, D. B., Pedersen, H. C., and Andersen, T. O. Speed-Variable Switched Differential Pump System for Direct Operation of Hydraulic Cylinders. In *Proceedings of the ASME/BATH 2015 Symposium on Fluid Power and Motion Control, Chicago, USA, October 14-16*. 2015.

Schneider, M., Koch, O., Weber, J., Bach, M., and Jacobs, G. Green Wheel Loader - Development of an energy efficient drive and control system. In *Proceedings of the 9th International Fluid Power Conference, Aachen, Germany, March 24-26*. 2014.

Skogestad, S. and Postlethwaite, I. *Multivariable Feedback Control - Analysis and Design*. Wiley, 2. edition, 2005.

Weber, J., Beck, B., Fischer, E., Ivantysyn, R., Kolks, G., Kunkis, M., Lohse, H., Lübbert, J., Michel, S., Schneider, M., Shabi, L., Sitte, A., Weber, J., and Willkomm, J. Novel System Architectures by Individual Drives. In *In Proceedings of the 10th International Fluid Power Conference, Dresden, Germany, March 8-10*. pages 29–62, 2016.

CC BY